AIP Publishing Applied Physics Reviews ACCEPTED MANUSCRIPT

This is the author's peer reviewed, accepted manuscript. However, the online version of record will be different from this version once it has been copyedited and typeset.

PLEASE CITE THIS ARTICLE AS DOI: 10.1063/5.0280969

The Enduring Legacy of Scanning Spreading Resistance Microscopy: Overview, Advancements, and Future Directions

Md Ashiqur Rahman Laskar[1±], Lennaert Wouters[2±], Pieter Lagrain[2], Jill Serron[2], Nemanja Peric[2], Andrea Pondini[2,3], Pierre Eyben[2], Thomas Hantschel[2], and Umberto Celano[1,2*]

[1] School of Electrical, Computer, and Energy Engineering, Arizona State University, Tempe AZ, 85281, USA

[2] imec, Kapeldreef 75, 3001, Leuven, Belgium

[3] KU Leuven, Department of Electrical Engineering, Kasteelpark Arenberg 10, 3001, Leuven, Belgium

± These authors equally contributed.

*Corresponding author: Umberto Celano, email: umberto.celano@asu.edu

Keywords: Scanning spreading resistance microscopy, Tomographic AFM, Scalpel SSRM, Carrier profiling, Failure analysis

ABSTRACT

Scanning spreading resistance microscopy (SSRM) has recently celebrated thirty years of existence when counting from the original patent of 1994. In this time the technique has experienced an incredible journey with substantial evolutions that transformed SSRM from a small-scale experiment into a staple for chips manufacturing laboratories for physical analysis of materials, failure analysis, and process development of integrated circuits. As the nanoelectronics industry is ready for a new inflection point, with the introduction of nanosheet field-effect transistor (NSFET) to replace FinFETs, and cell track scaling architectures such as the complementary field-effect transistors (CFET), SSRM is once again at a turning point. This review aims to highlight the state-of-the-art, while discussing the emerging challenges introduced by the ever-increasing complexity in complementary metal–oxide–semiconductor (CMOS) manufacturing. We start by illustrating the unique capability of the SSRM technique, its origin, and its evolution. Next,

AIP Publishing Applied Physics Reviews ACCEPTED MANUSCRIPT
This is the author's peer reviewed, accepted manuscript. However, the online version of record will be different from this version once it has been copyedited and typeset.
PLEASE CITE THIS ARTICLE AS DOI: 10.1063/5.0280969

we continue by showing the considerable research effort that enabled SSRM to transition to a tomographic sensing method in support of FinFET transistors. Here, the high aspect ratio fins geometry and the complex contacts technology have imposed important modifications to the original method. Later, we elaborate on some of the key challenges introduced by the upcoming device transition from three-sided channel FinFETs into nanosheet FET, i.e., offering a four-sided electrostatic control of the channel. Finally, we present the use of machine learning for automation in carrier calibration with increased accuracy. We close by introducing some of the concepts that we consider promising for further extension of SSRM to obtain sub-nm structural information, and doping profiles in the area of advanced FinFETs and nanosheet FET technologies, including (a.) correlatives analysis flow, (b.) liquid-assisted probing, and (c.) top-down and bottom-up multi-probe sensing schemes to merge low- and high-pressure SSRM scans.

Introduction

SSRM from the origin to state-of-the-art

At the dawn of sub-100 nm channel length planar metal-oxide field-effect transistor (MOSFET) technology, doping solutions such as ultra-shallow junction and halo implants were offering the only pathway to continue scaling the electrical logic switch.[1] The period in time was the early nineties, and the conventional methods for the extraction of carrier concentration (i.e., the concentration of electrically active dopants), such as spreading resistance profiling (SRP), and four-point probe (FPP), were facing insurmountable limits due to the new stringent probing conditions, i.e., high volumetric confinement for the region of interest.[2, 3] In addition, newly engineered junction profiles, designed with the support of modern electronic design automation (EDA) tools, required two-dimensional real-space imaging of the carrier profiles. This was key to monitoring new diffusion and activation problems often induced by new processes such as flash and laser annealing, epitaxially grown source/drain regions, which were clearly inaccessible to the available techniques.[4]

AIP Publishing Applied Physics Reviews ACCEPTED MANUSCRIPT
This is the author's peer reviewed, accepted manuscript. However, the online version of record will be different from this version once it has been copyedited and typeset.
PLEASE CITE THIS ARTICLE AS DOI: 10.1063/5.0280969

In parallel, those years marked the wide success of scanning probe microscopies (SPMs). With techniques that rapidly evolved from the complex operations of atomically resolved scanning tunneling microscopy (STM),[5] into a user-friendly analytical method such as atomic force microscopy (AFM)[6, 7], now available for virtually any type of material, and working in various environments including vacuum, inert atmosphere, and liquids.[8, 9] Soon after, the use of conductive probes rapidly paved the way to AFM methods that could sense electrical properties of the tip-sample junction, including current, capacitance, and far-field electrostatic phenomena.[10-12] Therefore, the work on SSRM was initiated in an attempt to merge well-known SRP and FPP with the enhanced probing capabilities offered by electrical AFM modes.[13]

SSRM is a secondary imaging mode of AFM operated in contact mode.[14-16] Here, a conductive probe is scanned at high pressure on the surface of a semiconductor with an applied electrical bias. While the feedback system of the AFM is used to maintain a high pressure between the probe and the surface (i.e., in the range of GPa), a logarithmic amplifier is used to collect the current flowing at the tip-sample junction. Given the high pressure required, classic metal-coated AFM probes tend to perform poorly and have a short lifetime. Therefore, almost immediately, the development of SSRM paired up with the development of conductive diamond probes. Given the reactive nature of the surfaces of semiconductor materials, the role of high tip-sample pressure is key to punching through any possible surface contamination layers, including native oxides, absorbed moisture, polymers, or soft residues, thus enabling a lowly-resistive contact (i.e., ideally ohmic), between the tip and the sample at the point of maximum pressure. The net result of all these considerations is that the tip-sample junction is now constituted of a fairly clean surface, where a scanning ohmic contact spreads a measurable electric current in a confined region inside the semiconductor material. The process of contact formation, and the overall quality of the tip-sample junction can be further promoted using vacuum, controlled atmospheres, or even liquids.

In addition, for various relevant semiconductor materials including Si, the tip-sample pressure has a special role as it promotes the formation of a phase transition from the semiconducting diamond phase to the metallic β-Sn phase.[17-19] Therefore, the localized

AIP Publishing Applied Physics Reviews ACCEPTED MANUSCRIPT
This is the author's peer reviewed, accepted manuscript. However, the online version of record will be different from this version once it has been copyedited and typeset.
PLEASE CITE THIS ARTICLE AS DOI: 10.1063/5.0280969

phase-changed metallic region in the vicinity of the probe acts as a highly confined metallic pocket in direct contact with the conductive tip. If represented in terms of an equivalent electric circuit, the loop is entirely constituted of resistive elements except for the junction created between the β-Sn pocket and the surrounding semiconductor material. Although counterintuitively, given the large size of the tip-contact region, SSRM uses the confinement of the spreading current between the β-Sn pocket and the surrounding material to enable high resolution imaging with the ability to sense features down to single digits nm.[20, 21] Moreover, as the measurement is dominated by the local spreading resistance, SSRM has access to quantitative information on the local resistivity. In general, the resistivity of a material is impacted by the presence of imperfections, such as defects, impurities, grain boundaries, etc. and in case of doped silicon by electron density and electron mobility.[22] Therefore, spreading resistance maps are first acquired, and later converted into 2D profiles with active carrier concentration. This is obtained by comparison with an epitaxially grown calibration standard (i.e., often looking like a staircase of layers with various doping levels) that is used for the calibration of quantitative electrical measurements. Importantly, given the Schottky nature of the tip-sample contact, the electrical response will be highly voltage-dependent, depending on the type and concentration of the dopants, thus it is key to maintain the same tip-sample bias conditions between the measurement and calibration. For an in-depth description of the physical mechanisms and detailed implementation of SSRM, multiple excellent sources exist.[23-25]

The desirable properties listed so far made SSRM a go-to solution in nanoelectronics for two- and three-dimensional carrier density mapping with high spatial resolution (ca. 1 nm), good dopant gradient resolution (1-2 nm/dec), and large dynamic range ($1E10^{15}$ – $1E10^{20}$ cm^{-3}), in a relatively inexpensive setup, and allowing for a flexible multi-sensing co-integration, i.e., where SSRM is added to other probing methods. **Figure 1** shows a mosaic with some of the main advancements in SSRM in the last decades. Far from being exhaustive, here we aim to emphasize the key role of diamond probe technology development, and the continued support of SSRM offered in the R&D phase of various CMOS architectures, which is obtained by placing side-by-side the evolution of these fields in the same period.

Applied Physics Reviews ACCEPTED MANUSCRIPT
AIP Publishing
This is the author's peer reviewed, accepted manuscript. However, the online version of record will be different from this version once it has been copyedited and typeset.
PLEASE CITE THIS ARTICLE AS DOI: 10.1063/5.0280969

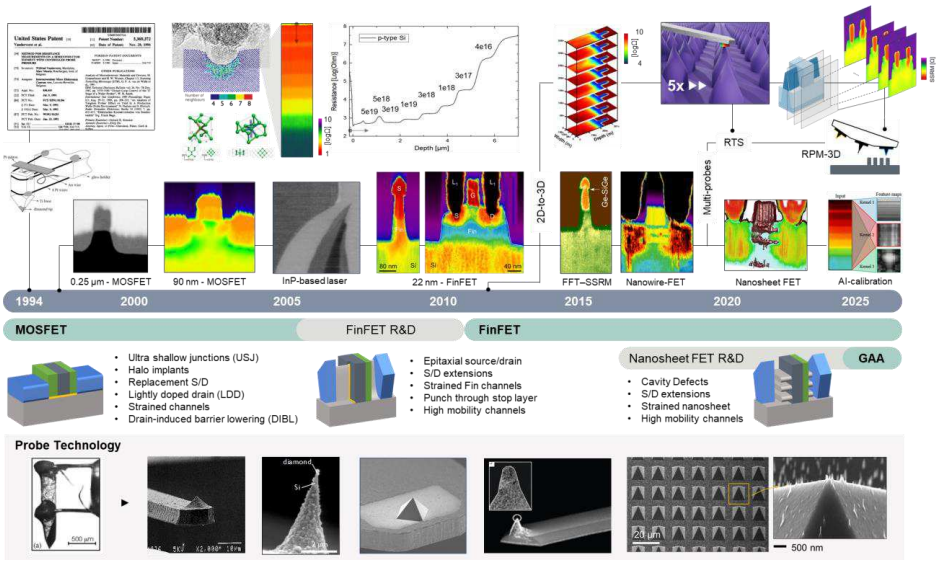

Figure 1: From the original patent application to modern day SSRM. Mosaic of the main steps in the evolution of the technique, with emphasis on its support in the development of CMOS process and failure analysis for MOSFET, FinFET, and nanosheet FET. The bottom panel reports on the fundamental advancements for conductive probes technology considered key in the embalmment of improved resolution, sensitivity, and repeatability for reliable SSRM measurements.

As described in the opening paragraphs, the lateral resolution and sensitivity of SSRM were never the intrinsic bottlenecks of the methodology, as no physical law limited ultra-scaled profiling and accurate carrier probing. However, diamond probe technology for high-pressure scans, the electronic limits of logarithm amplifiers, the integration with EDA tools, instrument design for site-specific localization, and extreme care to the sample preparation and measurement environment have driven the main areas of development for SSRM in the past years, and they still do in the present. Each of these areas of research will be discussed in a dedicated section of this review. First, we review the challenges faced by SSRM with the evolution of logic switches, i.e., transistors, as they

AIP Publishing Applied Physics Reviews ACCEPTED MANUSCRIPT
This is the author's peer reviewed, accepted manuscript. However, the online version of record will be different from this version once it has been copyedited and typeset.
PLEASE CITE THIS ARTICLE AS DOI: 10.1063/5.0280969

changed from planar MOSFET, to three-dimensional FinFET, and more recently, nanosheet FET. Second, the reader is introduced to the key modifications of conventional SSRM developed to remain relevant as devices were scaled and new materials introduced. These are among others, the soft-retrace, and fast-Fourier transform SSRM, with the addition of tomographic SSRM. Later, the wide range of emerging solutions is revised including, scanning in liquids and with multiple probes. Finally, the tremendous progress generated by probe technology is revised, discussing the key role of diamond probes for the SSRM community.

The MOSFET to FinFET transition

The rise of high-pressure AFM for material removal

If classic SSRM was introduced in support of junction profiling for planar transistors, the advent of FinFET technology forced the technique to progress in response to emerging challenges introduced by the new architecture. FinFET represents the first high-volume implementation of non-planar logic devices. Here, the transistor channel is raised above the silicon substrate, resembling a fin. The channel is surrounded on three sides by the oxide and metal gate while remaining attached to the Si substrate at the bottom side of the fin. Working practically as a fully depleted device, the entire channel region is depleted of charge carriers when the gate voltage is turned off. This means that there is no conducting path between the source and drain, resulting in very low leakage current. However, FinFET offers a much smaller volume of material in the channel for the SSRM technique to measure. Using geometrical considerations at the time of its introduction (i.e., 2011), the volume of the channel material for a single FinFET was less than 50% compared to the planar transistor counterparts. In addition, newly introduced epitaxially grown technologies to achieve increasingly higher dosages of dopants in combination with SiGe (in pFET) to generate stress and boost mobility in the S/D contacts, started to limit the sensitivity of SSRM in low-resistance range (i.e., high tip-sample currents).

AIP Publishing Applied Physics Reviews ACCEPTED MANUSCRIPT
This is the author's peer reviewed, accepted manuscript. However, the online version of record will be different from this version once it has been copyedited and typeset.
PLEASE CITE THIS ARTICLE AS DOI: 10.1063/5.0280969

Part of these limitations have been addressed with the introduction of fast-Fourier transform (FFT-SSRM) that enables the isolation of the local spreading resistance from the aforementioned parasitic resistance components.[26, 27] This is realized through force modulation at a controlled frequency, and the extraction of the resistance amplitude at this modulation frequency by performing an FFT-based lock-in deconvolution (here described in a dedicated section of this review). In addition, various reports addressed the major role that the environment played when performing SSRM, for example, using Ar, N, or high vacuum in the measurement chamber.[28-30] In essence, the reduction of the absorbed water layer on the sample surface improves the overall tip-sample junction resistance, offering improved resolution and sensitivity.[31] Finally, dedicated test structures available on chip inside metrology targets, allowed to improve the electrical connection of the back-contact by separating the S/D from the gate contacts. Therefore, through the combination of high-vacuum, FFT-SSRM, and an accurate focused ion beam (FIB) sample preparation, SSRM has successfully adapted to the requirements introduced by the advent of FinFETs.

Figure 2 shows an example of spreading resistance maps acquired on a Si-channel PMOS (FinFET) with a gate length (L_G) of 55nm where the sectional views of the spreading resistance profiles are reported in the region of the spacer (top), and in the body of the FinFET under the gate and contact (bottom). These images are generally interpreted in light of complementary electrical datasets, for example, drain current vs. gate voltage characteristics, analysis of peak conductance, studies on drain-induced barrier lowering (DIBL), or transfer length methods. Combining the 2D profiles of activated carriers with electrical data obtained from isolated devices or dedicated test-structures, is a powerful method to create a physical interpretation of the electrical results obtained from large area electrodes. Based on this methodology, multiple works reported the correlation between device performance (i.e., V_T roll-off, DIBL, and relationship between ON-current and S/D extensions, to name but a few) and carrier concentrations, investigating the role of epi growth in contacts, local interface resistances, doping diffusion and junction profiles in S/D regions for both Si- and Ge-channel devices.[32-35]

Applied Physics Reviews ACCEPTED MANUSCRIPT
AIP Publishing
This is the author's peer reviewed, accepted manuscript. However, the online version of record will be different from this version once it has been copyedited and typeset.
PLEASE CITE THIS ARTICLE AS DOI: 10.1063/5.0280969

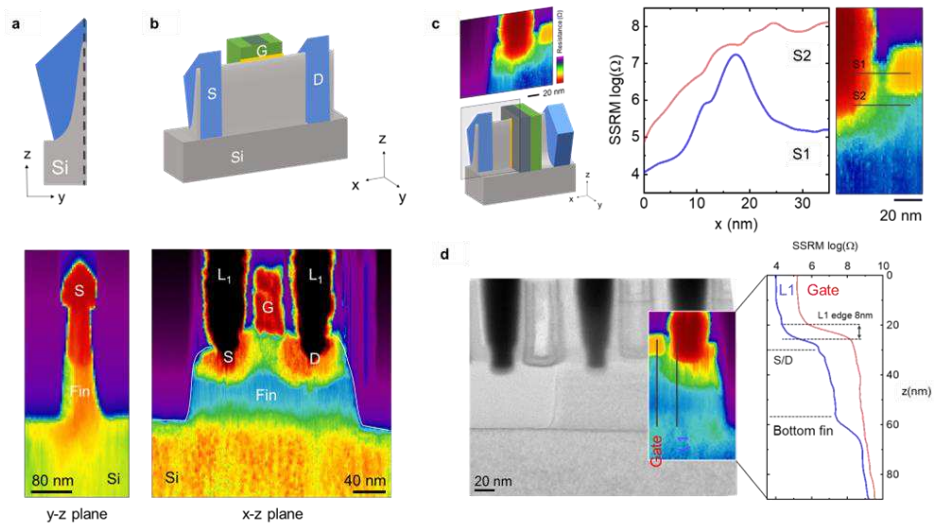

Figure 2: Characterization of a FinFET device Si-channel PMOS (FinFET) with gate length 55nm using SSRM. **a** and **b** show schematic representations of the FinFET structure in different orientations and corresponding SSRM maps. **c**. SSRM line profiles across the fin (x-direction) at two different locations (S1 and S2), highlighting the resistance variations in unit log(Ω). The inset shows the corresponding SSRM map. **d**. Cross-sectional transmission electron microscopy (TEM) image of the FinFET, with an inset showing the SSRM line profile along the fin height (z-direction) at the gate region. The profile reveals the resistance distribution from the source/drain (S/D) to the bottom fin.

Figure 2 demonstrates how SSRM can be used to visualize and quantify the electrical resistance distribution within the FinFET structure, providing insights into its performance characteristics. However, one of the most immediate problems introduced by FinFET is the intrinsic three-dimensional nature of the device, requiring a tomographic analytical capability in the area (i.e., volume) under investigation. The need to evolve SSRM into a tomographic method drove multiple attempts to extract SSRM data in 3D. Early works explored dedicated test vehicles including the use of staggered structures, and the

AIP Publishing Applied Physics Reviews ACCEPTED MANUSCRIPT
This is the author's peer reviewed, accepted manuscript. However, the online version of record will be different from this version once it has been copyedited and typeset.
PLEASE CITE THIS ARTICLE AS DOI: 10.1063/5.0280969

alternation between SSRM and focused ion beam (FIB) for a slice-and-sense analytical flow. While impactful, these exercises demonstrated additional complexity in the area of sample preparation and data interpretation.[36, 37]

An alternative approach is offered by the same mechanism used in SSRM to ensure a stable electrical signal and β-Sn phase formation, that is, the high tip-sample pressure. As discussed in the introduction, SSRM requires high tip-sample pressure to function. As a side effect of this high-pressure scan, the sample is progressively eroded, an effect traditionally considered as a drawback for the method as it makes the technique destructive (as reported in Supporting Information Figure S1). However, further studies on the possibility of controlling the high contact pressure to obtain a tunable material removal changed the original problem into an opportunity. The basic concept, often referred to as Scalpel SPM or tomographic AFM, is using the tip-induced material removal to achieve a slice-and-sense method where multiple SSRM profiles are collected at different probing depths and are finally interpolated into a 3D tomogram. Each of the key steps has been engineered over the years, as reported elsewhere.[38-41] Interestingly, since a material removal rate in the range of 1nm/scan can be obtained with the conventional tip-sample pressures employed in SSRM, performing both steps (a.) the removal, and (b.) the sensing, using one single tip, does not represent a major loss of resolution in 3D measurements when compared to a conventional 2D scan. This is a unique feature of SSRM, not observed when performing scalpel SPM with other electrical AFM modes, and it is enabled by the peculiar contrast mechanism of SSRM explained in the introduction.[42]

Particularly for non-planar architectures like FinFET, three-dimensional carrier density mapping is key to correlating the device performance with the manufacturing process. The use of scalpel SSRM tomographic reconstruction of S/D extensions and channel regions allowed to optimize the FinFET process development. **Figure 3** shows the progressive acquisition of an SSRM dataset for a Si-channel PMOS FinFET transistor with a channel length of 40 nm. The device under test is visible in Figure 3a using dark-field transmission electron microscopy (DF-TEM). The SSRM analysis is performed in the plane xz with the removal of material in the y direction, as shown in Figure 3b. From the visualization of the dataset in Figure 3c, it is clear that the volume contains one Si fin (i.e.,

Applied Physics Reviews ACCEPTED MANUSCRIPT
This is the author's peer reviewed, accepted manuscript. However, the online version of record will be different from this version once it has been copyedited and typeset.
PLEASE CITE THIS ARTICLE AS DOI: 10.1063/5.0280969
AIP Publishing

green SSRM contrast) contained inside an insulating SiO_2 layer (i.e., magenta SSRM contrast). All the structural elements contained in Figure 3a are now visible with their electrical response in the tomographic SSRM dataset, including the S/D regions, the gate, and the remainder of the SiO_2 used as a dielectric separation between adjacent fins. The removal rate can be estimated by dividing the number of 2D profiles collected before the complete erosion of the fin (i.e., fin width of 6 nm), here estimated (ca.) in range of 0.5 nm/scan. Given the high degree of precision in the erosion, it is possible to select individual SSRM planes for the detailed analysis of the features of interest, an example from the central part of the fin is shown in Figure 3d. The data presented in Figure 3 demonstrates the ability to obtain a set of slices for the complete volume of interest containing the channel of FinFET. While this is important to prove the ability of the scalpel SSRM to collect a complete dataset, in the majority of studies focusing on metrology for process development, the real advantage of this approach is its ability to slice throughout the volume of interest and stop when the FinFET channel is exposed. This enables the observer to acquire high-resolution SSRM profiles in selected regions of the device.

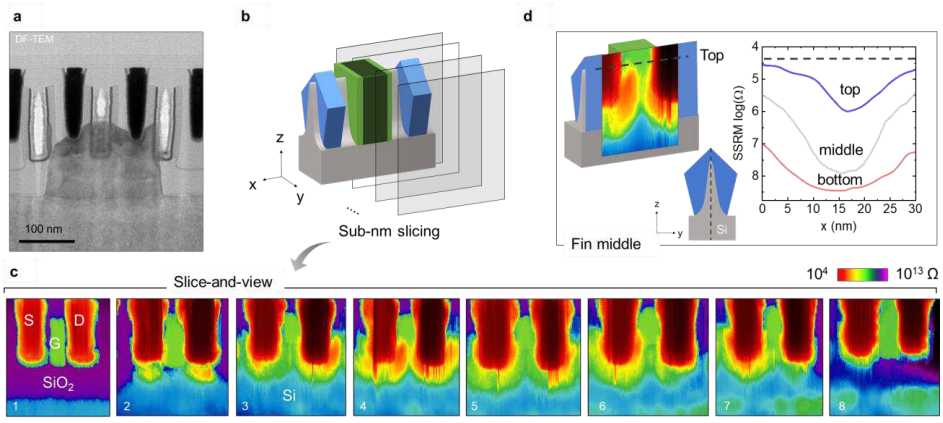

Figure 3: 3D characterization of a FinFET. **a**. Cross-sectional view of the FinFET structure, revealing the fins and gate for a transistor with 40nm channel length. **b**. The schematic depicts the "sub-nm slicing" approach, where the sample is conceptually sectioned into thin slices along the x-z plane. This is used to reconstruct a 3D view of the device. **c**. The "slice-and-view" panel presents a series of SSRM maps corresponding to

AIP Publishing Applied Physics Reviews ACCEPTED MANUSCRIPT
This is the author's peer reviewed, accepted manuscript. However, the online version of record will be different from this version once it has been copyedited and typeset.
PLEASE CITE THIS ARTICLE AS DOI: 10.1063/5.0280969

the individual slices obtained from the sub-nm slicing. These maps visualize the spreading resistance distribution within the FinFET structure, highlighting the source (S), drain (D), gate (G), and silicon dioxide (SiO_2) regions. The color scale represents SSRM resistance, with scan size of 200 x 200 nm^2. **d**. Detailed view and extracted 2D profiles from the SSRM image in the middle of the fin. This reveals the resistance variation across the fin at different vertical positions, providing insights into the device's electrical characteristics. The inset shows the location of the line profiles.

With the new paradigm of performing SSRM while slicing through a small volume, the control over nanoscale tip-induced material removal becomes crucial to enable an accurate probing of the volume of interest. While this remains an active area of research, multiple works reported on the comparison between different scanning parameters, analysis conditions, and environments for a sub-nm removal rate control. Clearly, the shape and radius of the apex are important parameters that, combined with the cantilever stiffness, play the major role in defining a homogeneous removal rate.[38, 43] Multiple considerations must be made also on the main scan parameters including scan speed, density of scan lines, and size of the scan area. It is observed that a correlation exists between the quality of the surface roughness in the machined area and the line density. Similarly, a tradeoff is observed between the maximum depth of the analysis crater and the analysis scan size, due to the formation of debris during the high-pressure scans that are not removed effectively from the area of interest.[38, 43-45] In addition, the simplified assumption of one homogeneous material undergoing tip-induced removal, is largely inaccurate when studying fully fabricated devices. **Figure 4** shows a schematic representation of a realistic case for FinFET where the probe is scanning over various types of materials during the same dataset. Here, the different removal rates between the shallow trench isolation (STI), i.e., oxide, and the metal gate region are causing morphological variations on the top surface that are often limiting the effectiveness of the SSRM measurement by introducing a preferential region for the removal to occur (as reported in Supporting Figure S2). Although a unique solution to this problem has not yet been identified, multiple alternatives exist to mitigate the effect, for example, soft-retrace

AIP Publishing Applied Physics Reviews ACCEPTED MANUSCRIPT
This is the author's peer reviewed, accepted manuscript. However, the online version of record will be different from this version once it has been copyedited and typeset.
PLEASE CITE THIS ARTICLE AS DOI: 10.1063/5.0280969

SSRM (SR-SSRM), which reduces the tip-sample pressure on one of the two passages along the fast-scan axis, has the objective to minimize the impact of metal smearing.[46] Alternatively, the tip-sample pressure could be dynamically adjusted based on morphological considerations, to minimize the insurgence of uneven removal regions. This can be achieved with a dedicated multi-probe sensing scheme (as discussed later in this review).[47] Noteworthy, various reports indicate that the use of liquid environments, where the probe operates while immersed in a liquid solution, has a major impact on the removal of debris thanks to the reduced surface tension and the enhanced desorption of residual particles.[44] In addition, when using inert liquids like oil, functional electrical SSRM could be performed with minor variations compared to a classic dry experiment (as discussed later in this review). Finally, the use of chemically active wet environments can also promote the effective removal of material, as previously reported in alternative AFM methods.

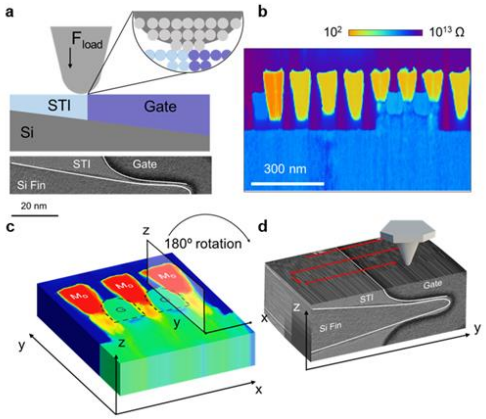

Figure 4: Schematic of Scalpel SSRM in the presence of multiple materials. **a**. The probe is scanning on **a**. Si-channel of a FinFET. Thus, both oxide and metallic layers are separating the probe from the Si Fin before the material removal starts. **b**. Large area SSRM measurement of the area of interest, multiple dummy contacts are visible near the Si Fin. Note, in the fin region the gates are not connected to the back-contact, thus the gate metal does not present the same contrast as the other contacts. **c**. Three-dimensional view of the active area with three (S/D) contacts indicated by M_0 and two

AIP Publishing Applied Physics Reviews ACCEPTED MANUSCRIPT
This is the author's peer reviewed, accepted manuscript. However, the online version of record will be different from this version once it has been copyedited and typeset.
PLEASE CITE THIS ARTICLE AS DOI: 10.1063/5.0280969

gates. **d**. Schematic showing the actual scanning direction as the probe approaches the core of the Fin region.

Heavily doped S/D epitaxy and the need for FFT-SSRM

Overcoming parasitic resistance components

With the advent of S/D engineering impacting composition, strain, electronic defects and epi-layers doped at increasing dosages of B, P, and As, SSRM started to show evident limitations for the quantitative analysis of active carriers in S/D contacts, as well as in the channel region. The origin of the problem was to be found in the very nature of the data acquisition for SSRM. Here, the fundamental condition for a quantitative estimate of carrier concentration requires the tip-sample junction spreading resistance to dominate over the other resistive terms of the tip-to-ground electrical connection. This is due to the fact that the R_{total} measured in SSRM is sensitive to the voltage divider established in the tip-to-ground equivalent circuit, thus requiring $R_{spreading}$ to be at least one order of magnitude larger than any other elements for the R_{total} to reflect the underlying resistivity property of the material (as reported in Supporting Information Figure S3). However, the non-perfectly Ohmic SSRM tip-sample nanocontact $R_{contact}$, and the influence of parasitic resistances such as the resistance of probe R_{probe}, the bulk sample resistance R_{bulk}, and the back-contact resistance $R_{back\text{-}contact}$, interfere with the targeted spreading resistance $R_{spreading}$:

$$R_{total} = R_{spreading} + R_{contact} + R_{probe} + R_{bulk} + R_{back-contact}$$

The contact resistance is dramatically suppressed by the formation of the metallic beta-tin phase of silicon under the high tip load force. However, a residual Schottky barrier resistance remains due to the nature of the materials involved in the SSRM nanocontact (a diamond probe, the beta-tin phase of silicon, and the silicon sample), none of which are true metals. The intrinsic probe resistance itself is minimized through the use of highly boron-doped diamond tips, but it is non-zero, which becomes particularly limiting in low-

AIP Publishing Applied Physics Reviews ACCEPTED MANUSCRIPT
This is the author's peer reviewed, accepted manuscript. However, the online version of record will be different from this version once it has been copyedited and typeset.
PLEASE CITE THIS ARTICLE AS DOI: 10.1063/5.0280969

resistive regions, such as the heavily doped S/D contacts in FinFET devices (as reported in Supporting Information Figure S3). Moreover, with decreasing device dimensions, focused ion beam milling and Pt deposition became vital for back contact preparation, thus adding the risk of the sample surface interacting with the energetic Ga beam introducing an additional amorphous layer between the sample and the deposited Pt, which adds a back-contact resistance component. At the same time, smaller devices will lead to geometrical confinement of the current, introducing an additional bulk resistance component for the current to flow to the back-contact. Therefore, the cases where $R_{spreading}$ is no longer dominant started to increase, impacting the quantification of data, with large distortions as visible in **Figure 5**c,d. [26] Clearly, this problem affects multiple devices, including FinFETs, nanosheet-FET, or high-aspect-ratio vertical channels used in memory applications, hindering the use of SSRM.

To overcome this limitation, researchers embarked on a substantial technical modification of the technique, which was named fast Fourier transform scanning spreading resistance microscopy.[26, 27] FFT-SSRM enables the isolation of the local spreading resistance from the aforementioned parasitic resistance components. This is realized through force modulation at a controlled frequency, and the extraction of the resistance amplitude at this modulation frequency by performing an FFT-based lock-in deconvolution (Figure 5a,b). The key to the success of the technique lies in the dependency of the β-Sn pocket size, and thus the spreading resistance, on the applied force, whereas parasitic resistance components remain force-independent. As a result, the modulation in the measured resistance originates exclusively from the spreading resistance, enabling a direct relationship to the local resistivity and carrier concentration.

Applied Physics Reviews ACCEPTED MANUSCRIPT
This is the author's peer reviewed, accepted manuscript. However, the online version of record will be different from this version once it has been copyedited and typeset.
PLEASE CITE THIS ARTICLE AS DOI: 10.1063/5.0280969
AIP Publishing

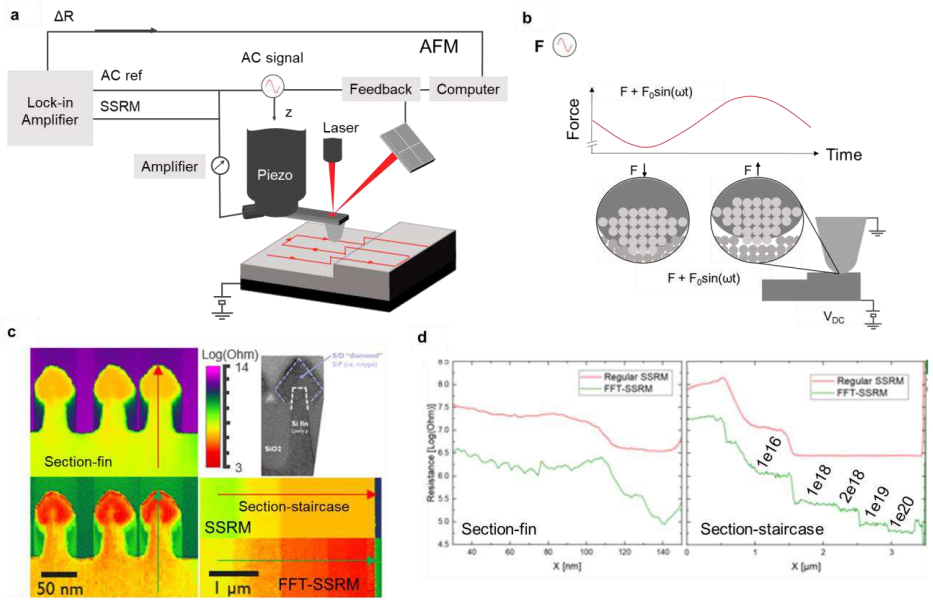

Figure 5: FFT-SSRM. **a**. Diagram FFT-SSRM setup, where a lock-in amplifier decouples the spreading resistance from parasitic series resistances by applying an AC voltage signal to the AFM z-piezo, thereby modulating the force on the cantilever. **b** Schematic of the fundamental principle of operation for FFT-SSRM. **c** Comparison of regular SSRM and FFT-SSRM imaging and **d** profiles**,** for FinFET S/D regions an epitaxially-grown staircase calibration structure (imec) with a 3 MOhm resistor added in series. The comparison of resistance profiles for both samples demonstrates improved doping contrast enabled by FFT-SSRM.

The value of FFT-SSRM is demonstrated in Figure 5c,d, by a comparative study with regular SSRM on an n-type doped Si staircase sample with a resistor of 3 MOhm added in series. In the regular SSRM measurement, highly doped layers (≥ 1e18 carriers/cm^3) cannot be distinguished since the actual spreading resistance is screened by the series resistance. Consequently, the carrier concentration calibration in this regime is not possible anymore. In the FFT-SSRM measurement, however, the spreading resistance

AIP Publishing Applied Physics Reviews ACCEPTED MANUSCRIPT
This is the author's peer reviewed, accepted manuscript. However, the online version of record will be different from this version once it has been copyedited and typeset.
PLEASE CITE THIS ARTICLE AS DOI: 10.1063/5.0280969

contrast is preserved, thus calibration opportunities remain. Note that the artificially added series resistance in this showcase example can be representative of any sort of parasitic resistance. This demonstration validates that the FFT-SSRM method successfully isolates information related to the spreading resistance and hence the local carrier concentration from undesired series resistance components, thereby enabling excellent sensitivity over the entire carrier concentration range of interest. A real-life process control application is added in Figure 5b, which illustrates the electrical characterization of in-situ doped Si:P S/D diamonds epitaxially grown on bulk Si fins. The confined volume of the fins and the S/D regions adds significant resistance to the current trajectory toward the back-contact, located a few hundred nanometers away from the measured cross-section plane, causing the SSRM resistance to saturate at approximately 7MOhm. However, due to the application of the FFT-SSRM concept, it was possible to retrieve information about the local carrier density profile within the S/D diamonds. This application demonstrates that FFT-SSRM extends spreading resistance-based carrier profiling to nanometer-scale 3D devices, enabling more accurate profiling, especially in structures with parasitic resistances.

Other examples of the use of FFT-SSRM to limit the loss of sensitivity due to tip resistance for highly doped samples, avoid the grain boundary-induced series resistance in poly-Si grains, improve resistance contrast in the gate stack of DRAM periphery p-MOSFET structures, or significantly enlarge the dynamic range in non-Si materials, were presented in previous works.[27, 48]

The era of nanosheet FET

3D-carrier Profiling in Vertically Stacked Nanosheets

Thanks to the previous sections the reader should be able to understand the large transformations that enabled SSRM to evolve from a technique limited to long channels planar transistors to FinFETs and non-planar logic devices. Nonetheless, as the interest of the industry is moving towards architectures such as nanosheet FET, SSRM finds itself

AIP Publishing Applied Physics Reviews ACCEPTED MANUSCRIPT
This is the author's peer reviewed, accepted manuscript. However, the online version of record will be different from this version once it has been copyedited and typeset.
PLEASE CITE THIS ARTICLE AS DOI: 10.1063/5.0280969

once more at the crossroads of emerging developments to surmount novel challenges. Nanosheet FETs present many similarities with FinFETs in their manufacturing process, but differ significantly in the formation of multiple vertically stacked nanosheets that constitute a type of transistor channel electrostatically controllable on four sides (Figure 1).[49, 50] The higher degree of electrostatic control, geometrically set modulation of the ON-currents, good scalability, and improved OFF-currents have made nanosheet FETs the frontrunner to replace FinFETs, and at the time of writing, their commercialization with high volume production is imminent.

Among the most complex characterization tasks for a nanosheet FET is the accurate analysis of S/D contacts after the channel release step. At this stage, the nanosheet channels have been epitaxially grown, and the inner spacers are formed to isolate the gate from the source and drain regions. SiGe layers are selectively etched away, releasing the silicon nanosheets to form the channel structures. After the replacement metal gate is integrated, the epitaxial growth of the source/drain material is performed. This critical step requires precise control to avoid damaging the delicate nanosheets while creating the low-resistive contact between each nanosheet and the S/D material. For this reason, the impact of doping diffusion in the nanosheets, and the role of defects in S/D epi with novel cavity-filling processes must be studied to improve device performance.

However, when considering the current spreading into what is left of the Si nanosheet after the channel region has been made accessible to the AFM probe, it is clear that the basic physics of SSRM is no longer applicable. **Figure 6** shows dimensions for a fully integrated nanosheet FET. Although dimensions will likely vary, an individual nanosheet is expected to have a length of 20-30 nm with a sheet geometry resembling a rectangle with sides of ca. 8 x 20 nm. Recent studies reported on the deviation of SSRM from the expected results when studying ultra-confined Si in a silicon-on-insulator wafer. The choice of the sample enabled the experiments to show the progressive increase of SSRM resistance as a function of the sample's thinning. Here, as the current is all confined within the Si layer, this experiment provides a measure of the effect of the Si thickness on the SSRM measurements. One of the main findings is the fact that the charge transfer phenomena in the buried interface Si/SiO_2 can play a major role in the confinement of the

AIP Publishing Applied Physics Reviews ACCEPTED MANUSCRIPT
This is the author's peer reviewed, accepted manuscript. However, the online version of record will be different from this version once it has been copyedited and typeset.
PLEASE CITE THIS ARTICLE AS DOI: 10.1063/5.0280969

spreading current to the point that when the Si slab is thinner than 10 nm interface traps and carrier concentration blends into a complex term to disentangle with severe limitations to the SSRM quantification.[51]

Figure 6 shows the nanosheet FET structure under test, with details on the module integration using TEM, and SSRM results in Figure 6b. While SSRM can sense each of the elements visible in Figure 6a, the presence of the metal gate covering the nanosheets hinders the observation of the channels. Using the scalpel SSRM, the presence of the nanosheet can be revealed (Figure 6c), and by means of soft-retrace SSRM, the resolution in the nanosheet regions can be further improved, at the expense of quantitative reconstruction. While the reduced tip-sample contact area in SR-SSRM enables higher resolution, the lack of high-pressure reduced the reliability of this method for the carrier quantification, thus running the experiment in a regime that is closer to a conductive AFM (C-AFM) experiment. Other experiments on similar structures are reported in Supporting Information Figure S4.

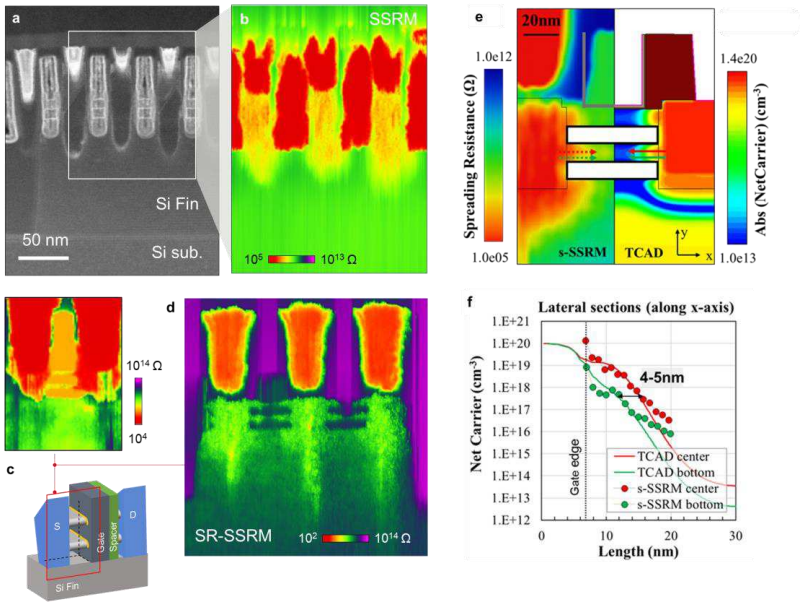

AIP Publishing Applied Physics Reviews ACCEPTED MANUSCRIPT
This is the author's peer reviewed, accepted manuscript. However, the online version of record will be different from this version once it has been copyedited and typeset.
PLEASE CITE THIS ARTICLE AS DOI: 10.1063/5.0280969

Figure 6: Characterization of a Nanosheet FET structure using SSRM. **a**. Transmission electron microscopy image showing the device structure in the area where SSRM is performed. **b**. Associated SSRM image revealing the resistance map. **c**. Schematic of the channel region with details of SSRM and **d**. Soft-retrace SSRM is used here to increase the sensitivity to the channel regions (note: Gate metal was not back-contacted, therefore no current flow and high resistance in SSRM map.). **e**. Comparison between the two-dimensional TCAD carrier map and the s-SSRM resistance map. **f**. Comparison between TCAD and s-SSRM carrier sections along the x-axis in the center and on the bottom side of the bottom nanowire from the SiGe-Si interface. (Figure 6e-f are Reproduced with permission from *2021 20th International Workshop on Junction Technology (IWJT)*, Kyoto, Japan, 2021, pp. 1-4., Copyright 2021 The Institute of Electrical and Electronics Engineers)

SSRM for failure analysis and TCAD calibration

Technology Computer-Aided Design (TCAD) tools represent a branch of Electronic Design Automation (EDA) and utilize computer simulations with physics-based models to develop and optimize semiconductor device technology. TCAD tools have been employed since the late 1960s (mainly one- and two-dimensional simulators modelling bipolar devices), although the real emergence of TCAD tools was in the 1980s, with the advent of CMOS logic microprocessors. Two-dimensional process and device simulators have been utilized intensively to experiment virtually different processing steps and determine the best possible options prior to fabrication. Hence, laborious and expensive experimental explorations were replaced by TCAD simulations, which are less time-consuming and often more insightful.

The models included in TCAD tools have been calibrated for years using metrology data, with one-dimensional characterization techniques (such as SIMS or SRP among others) commonly used. However, calibrating two-dimensional models with one-dimensional data is often not the most reliable approach, making SSRM very useful for the calibration of TCAD tools since the early 2000s. It began in 2004 with process simulator calibration on a 90nm n-MOSFET[52] that emphasized the ability of SSRM to

AIP Publishing Applied Physics Reviews ACCEPTED MANUSCRIPT
This is the author's peer reviewed, accepted manuscript. However, the online version of record will be different from this version once it has been copyedited and typeset.
PLEASE CITE THIS ARTICLE AS DOI: 10.1063/5.0280969

probe finer details of the two-dimensional carrier distribution within the channel area, imaging the impact of the halo and V_T-adjust implants. Comparisons of the lateral extent of the halo-profiles between SSRM and simulations could demonstrate that the simulations underestimated the lateral width of the halo-profiles, while the vertical depth was consistent with the SSRM carrier maps. Quantitative comparisons of channel profiles taken on large structures also indicated a difference in absolute concentration between SSRM and simulations, highlighting the need for TCAD two-dimensional calibration. Results were also published for 65nm [9] and 45nm technological nodes, as well as for High Speed SiGe:C Heterojunction Bipolar Transistors (HBTs)[53].

As discussed in the previous section, in FinFET devices, even the smallest variations of the structure dimensions (i.e., width or length, local interconnect or spacer, source/drain epi volumes, etc.), carrier distribution and/or activation rate can cause significant variations in the electrical properties. This leads to the intensified need to come up with properly calibrated three-dimensional process and device simulation tools to predict performances, suggest processing options and even understand failure mechanisms. And once again, SSRM appears to be a unique and very useful tool for this scope. SSRM has been performed on various three-dimensional devices for failure analysis. Here, metrology data extracted from two- and three-dimensional SSRM carrier maps in combination with other techniques such as TEM (displaying epi shape and volume, fin or nanowire size) or EDS (showing epi composition in source/drain), has great value for the calibration of TCAD decks. This approach was used for the simulation of Si-channel FinFET devices[46], for instance pointing out the impact of remaining oxides after pre-epi clean in n-FinFET, or of Ge content in SiGe epi S/D on the access resistance in p-FinFET. A simulation deck for the Nanowire pFET device was also implemented, analyzing the impact of reduced carrier diffusion in the nanowires on device performance. In **Figure 6**e,f, one can, for instance, observe the good correspondence obtained between s-SSRM results and TCAD simulations (including the impact of gate oxide proximity on the diffusion inside nanowires). All these results are collected and discussed in more details elsewhere.[32]

AIP Publishing Applied Physics Reviews ACCEPTED MANUSCRIPT
This is the author's peer reviewed, accepted manuscript. However, the online version of record will be different from this version once it has been copyedited and typeset.
PLEASE CITE THIS ARTICLE AS DOI: 10.1063/5.0280969

SSRM beyond nanoelectronics

Uses for emerging III-V materials and solar cells

Traditionally used for the characterization of ultra-scaled transistors and process development for advanced CMOS technologies, SSRM has found increasing utility in other fields, including solar cells, photonic devices, image sensors, and Si power transistors. [23, 54-57] These areas leverage silicon's versatility when doped and they require precise electrical characterization at the nanoscale, making SSRM a valuable tool for optimizing performance and understanding critical device properties. **Figure 7** illustrates the SSRM analysis results of silicon solar cell samples to investigate (a) the impact of a nickel immersion plating metallization step on the doping profile in the underlying heavily doped emitter layer. Here, creating a good electrical contact between the metal grid and the silicon emitter is essential for achieving a low contact resistance, which minimizes power losses in the solar cell. (b) The 2D carrier profile in periodic inverse nanopyramid textured surfaces, and (c) the annealing effect on enhanced dopant diffusion through pinholes in ultrathin SiO_x films for poly-Si passivating contacts were also studied.[56] Integrated optics is another technology with a wide range of applications, playing a vital role in modern communication, sensing, and information processing. Waveguides enable the integration of various optical functions onto a single chip, similar to electronic integrated circuits. In both cases, SSRM provides a valid characterization method for the assessment of the local concentration. Figure 7d shows the 2D SSRM resistance map of a pn silicon waveguide structure which was used to calibrate simulation results for the device performance due to its strong correlation to doping concentration.

AIP Publishing Applied Physics Reviews ACCEPTED MANUSCRIPT
This is the author's peer reviewed, accepted manuscript. However, the online version of record will be different from this version once it has been copyedited and typeset.
PLEASE CITE THIS ARTICLE AS DOI: 10.1063/5.0280969

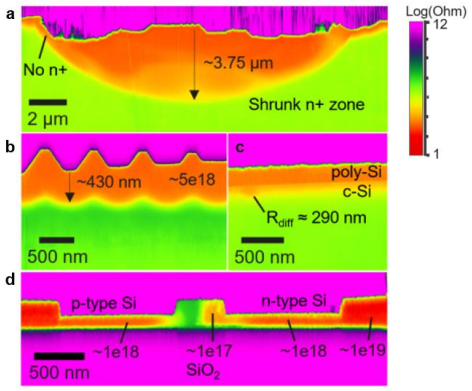

Figure 7: SSRM applied to solar cell samples. **a**. SSRM analysis of the electrical contact between the metal grid and the silicon emitter, creating low contact resistance. **b**. The 2D carrier profile in periodic inverse nanopyramid textured surfaces and **c**. SSRM analysis of the annealing effect on enhanced dopant diffusion through pinholes in thin SiO_x films for poly-Si passivating contacts. **d**. Junction observation in solar cell sample.

In recent years, the growing integration of non-Si materials, such as Ge, III-V compounds, and SiC, has further expanded the scope of SSRM applications. This shift is driven by the increasing adoption of these materials in areas where they dominate due to their superior performance characteristics, such as power devices, high-frequency applications, and photonics.[54, 58, 59] Clearly, most of the SSRM fundamental physics is based on the unique response of Si under the application of a highly confined load i.e., the formation of the β-Sn pocket. However, studies have also reported the formation of a β-Sn pocket in germanium.[60] Therefore, extensive research into the properties of the β-Sn pocket has significantly contributed to advancing the understanding and application of SSRM to germanium with the realization that the abundant presence of surface states on the Ge surface (i.e., cross-section) reduces the sensitivity of SSRM substantially when compared to Si.

AIP Publishing Applied Physics Reviews ACCEPTED MANUSCRIPT
This is the author's peer reviewed, accepted manuscript. However, the online version of record will be different from this version once it has been copyedited and typeset.
PLEASE CITE THIS ARTICLE AS DOI: 10.1063/5.0280969

For III-V materials, the β-Sn phase does not exist, and hence, no detailed information on the exact size and shape of the nanocontact is yet available. Despite this, several materials show a strong non-linear resistance vs. force curve, often linked to a pressure-induced phase transition. Even in absence of a clear pressure-induced phase transition, the use of large tip-sample bias can be used to electrically punch through the potential of the Schottky contact under the probe. Measurements on dedicated test structures reveal that dopant variations can be distinguished by the related spreading resistance values, however, the sensitivity is generally lower as compared to Si. Consequently, the applicability of SSRM on III-V materials is mostly determined empirically, using staircase structures or devices.[48, 61, 62] For instance, Xu et al.[63] have studied the tip-sample nanocontact to InP in detail in order to make measurements on this material. Compared to Si, InP is a soft material with different mechanical properties requiring a reduced load force to perform SSRM. Indeed, probing InP at standard SSRM load force induces physical removal of the material, which has been exploited to probe the conductivity of the sample at different depths.[63] In addition, the strong tendency of InP to get oxidized at ambient conditions limits the possibility to perform repeated SSRM scans with metal tips and low forces. Over the years, with the help of vacuum and controlled environments, SSRM has been demonstrated on InP and other III-V materials, enabling important observations in the field of photonic, batteries and RF-devices.[61, 64, 65] Figure 8 shows a 2D SSRM resistance map of a GaAs nano-ridge PIN laser diode structure and the resistance maps of the p- and n-GaAs calibration samples, featuring multiple layers with known carrier concentrations. The SSRM measurement successfully visualizes the differently doped regions in the nano-ridge with high resolution and allows to extract the active carrier concentration for every region using the corresponding calibration measurements. This information is used to get a better fundamental understanding of the influence of growth conditions on the resulting stack or to validate model predictions of electrical characteristics and therefore is valuable feedback in the process development of these GaAs nano-ridge laser diodes.[66] Importantly, for this type of application, the ability to acquire more than one single voltage condition can be beneficial for the in-depth inspection of the SSRM response in the area under study. Recent work on force-volume

Applied Physics Reviews ACCEPTED MANUSCRIPT
AIP Publishing
This is the author's peer reviewed, accepted manuscript. However, the online version of record will be different from this version once it has been copyedited and typeset.
PLEASE CITE THIS ARTICLE AS DOI: 10.1063/5.0280969

hyperspectral SSRM imaging has demonstrated this functionality in a wide range of biases, often referred to DataCube-SSRM.[67]

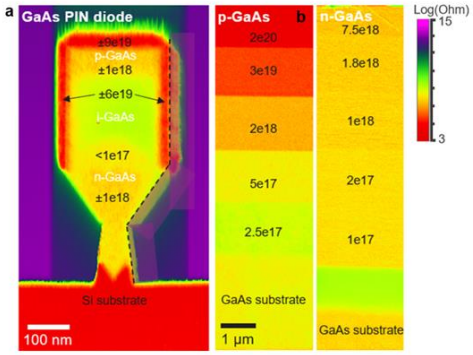

Figure 8: SSRM applied to on-chip photonic. **a**. Details of GaAs nano-ridge laser diodes with SSRM. **b**. GaAs epitaxially grown calibration structures used for quantitative SSRM measurement in non-Si materials.

Finally, SSRM has also been applied to investigate the electrical properties of GaN-based devices. However, due to GaN's wide bandgap and high hardness, SSRM measurements face challenges such as a high tip-sample contact resistance, non-ohmic back-contacting, and the difficulty in preparing smooth, damage-free cross-sections for accurate measurements. Despite these challenges, SSRM has proven effective for characterizing heavily doped regions and analyzing device behavior in GaN-based power devices.[68, 69] These examples demonstrate the strength of SSRM beyond CMOS logic, extending to any silicon- or non-silicon-based technologies where doping distributions matter. Moreover, the typically more relaxed device dimensions in these applications significantly reduce the complexity of the SSRM analysis.

Active Dopant Concentration

Reliability and limits of SSRM calibration in real case studies

AIP Publishing Applied Physics Reviews ACCEPTED MANUSCRIPT
This is the author's peer reviewed, accepted manuscript. However, the online version of record will be different from this version once it has been copyedited and typeset.
PLEASE CITE THIS ARTICLE AS DOI: 10.1063/5.0280969

Based on the various examples and spreading resistance maps (2D and 3D) from the previous sections, there can be the misleading assumption that SSRM can enable the quantitative sensing of active carriers in every situation. However, the quantitative extraction of active dopant concentration using SSRM is a broad research topic that goes back to the origin of the technique and has had important developments over the course of the years.[70] Also, it is important to recognize some of the implications and limitations imposed by the fact that SSRM remains a two-probe-based electrical method, thus intrinsically plagued by the limitations of these techniques.[71]

The SSRM technique enables the extraction of quantitative information on the active carrier concentration within semiconductor materials through the intrinsic relationship between the measured spreading resistance and the local resistivity of the probed material:

(1) $Rsp = \frac{\rho}{4a}$

where a is the electrical tip radius and ρ is the material resistivity. Importantly, equation 1 is only valid when the electrical radius (a), is large compared to the mean free path (λ) of electrons and holes. However, in practice, several factors complicate the straightforward resistivity calculation, the main reason being the uncertainty about the exact tip size. Additionally, the influence of the parasitic tip-sample contact, probe, bulk, and back-contact resistances, discussed in detail in an earlier section, further obstructs the direct quantification from this formula.[51] Finally, it is worth mentioning that ballistic Sharvin equation is more accurate compared to equation 1 in those cases where lowly-doped material exhibits mean free path of larger than 10 nm.[51] To address these challenges, the SSRM quantification relies on experimental calibration curves. These calibration curves are obtained from measurements on specially designed calibration samples, which are epitaxially grown structures comprising multiple layers with uniform and precisely known resistivity values. Importantly, these calibration measurements are conducted under the same experimental conditions (e.g., tip, applied load force, and sample bias) as those used in the SSRM analysis of the sample of interest. This

AIP Publishing Applied Physics Reviews ACCEPTED MANUSCRIPT
This is the author's peer reviewed, accepted manuscript. However, the online version of record will be different from this version once it has been copyedited and typeset.
PLEASE CITE THIS ARTICLE AS DOI: 10.1063/5.0280969

consistency assures that deviations in probe and contact resistances between the calibration and sample measurements are effectively eliminated. To minimize bulk resistance, attention is given to the series resistance along the current path to the back-contact ($R = \rho \cdot \frac{L}{A}$). This can be achieved by either ensuring a large area or a low-resistivity current path or using a focused ion beam (FIB) to place the back-contact as close as possible to the measured cross-section, thereby reducing the current path length.[72] Finally, the contribution of back-contact resistance is mitigated by establishing the formation of a (near) ohmic contact. When the contact must be realized directly on silicon (e.g., in a calibration or any other blanket sample), GaIn eutectic is the preferred back-contact material. In case of fully processed devices, the metal-one (M1) or back-end metal layers connected to the fabricated device contact plugs (e.g. S/D and gate contacts) can be used to drain the current, with FIB assistance if needed. By applying all these measures to both the calibration sample and the sample of interest, the measured resistances in the various layers of the calibration sample can be reliably used to calibrate the resistivity of the unknown sample.

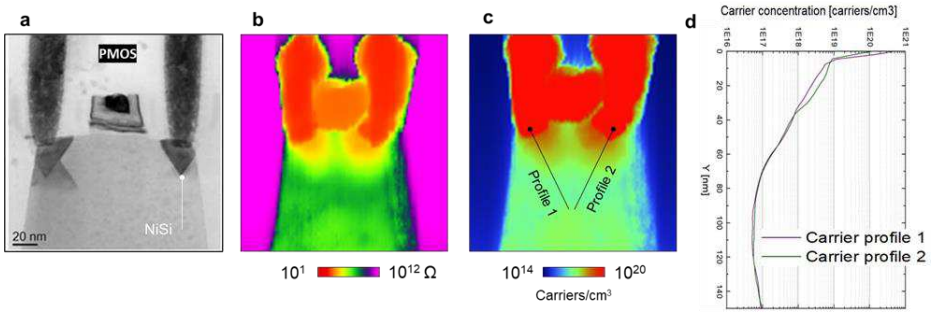

Figure 9: Quantified SSRM workflow. **a**. STEM image of the area under test. **b**. SSRM resistance map of the well implant in a 28 nm planar PFET device. **c**. The boron diffusion in source/drain implants and the well implant is quantified to estimate the 2D map of carrier concentration and line profiles as shown in **d**.

AIP Publishing Applied Physics Reviews ACCEPTED MANUSCRIPT
This is the author's peer reviewed, accepted manuscript. However, the online version of record will be different from this version once it has been copyedited and typeset.
PLEASE CITE THIS ARTICLE AS DOI: 10.1063/5.0280969

The quantitative SSRM data processing workflow is illustrated in Figure 9. It is applied here to estimate the carrier concentration and analyze the boron diffusion in source/drain implants and determine the junction depth to the well implant in a 28 nm planar PFET device. The SSRM resistance measurement of a p-type doped silicon staircase calibration sample is shown in Supporting Information Figure S5. Average resistance values for the different layers are retrieved from the measurement to construct a calibration curve, which represents the relationship between resistance and carrier concentration. This calibration curve is subsequently used to convert the resistance map of the PFET device, measured with the same experimental conditions, into its carrier concentration map (Supporting Information Figure S5). The extracted carrier profiles reveal a peak doping concentration of 1×10^{19} carriers and indicate boron diffusion extending up to approximately 90 nm from the NiSi source/drain contacts, where the junction with the well implant is located (Figure 9c,d). Theoretically, the carrier concentration at the junction should go down to the intrinsic level (~$1x10^{10}$ atoms/cm^3), however, leakage currents induced by the applied tip-sample bias compromise the accurate carrier quantification within the junction. Reducing the sample bias can provide more reliable information on the carriers near electrical junctions and on the junction depth.

From the calibration measurement, it is evident that the SSRM technique covers a wide dynamic range in silicon. However, at lower doping levels, the measurement is limited by the influence of surface states, associated with dangling bonds present on the surface. [2, 73] These surface states begin to dominate over the bulk carriers at doping levels from $1e^{15}$-$1e^{16}$ carriers/cm^3 and below, with the exact transition depending on the chosen cross-section preparation method (e.g., cleaving or polishing with or without post-UV treatment, chemical passivation, or thermal annealing). Since silicon surface states act as n-type carriers, the characteristic junction resistance peak associated with electrical junctions disappears for n+p junctions, rendering SSRM insensitive to such junctions. At the higher doping levels, the SSRM measurement is constrained by the probe resistance. For regions with doping concentrations on the order of $5e^{20}$ carriers/cm^3, the probe resistance (typically ~1 kΩ for highly boron-doped diamond tips) becomes dominant over the spreading resistance. The fingerprint of the probe resistance is recognized as a

AIP Publishing Applied Physics Reviews ACCEPTED MANUSCRIPT
This is the author's peer reviewed, accepted manuscript. However, the online version of record will be different from this version once it has been copyedited and typeset.
PLEASE CITE THIS ARTICLE AS DOI: 10.1063/5.0280969

flattening in the calibration curve, this is the indication that the resistance values at play are no longer measurable with conventional SSRM, as it can be observed in Figure 9. The use of FFT-SSRM can further extend the dynamic range at the high doping side. Note that accurate carrier quantification is restricted to the range of the calibration sample in use, i.e. $4e^{16}$-$5e^{19}$ carriers/cm^3 in this example.

Other factors that can hinder quantitative SSRM include the use of FIB for cross-section preparation and situations where the region of interest (ROI) is confined to a limited volume. For many sub-100 nm devices, the use of FIB is essential for exposing the ROI on a sample cross-section. The energetic ions drastically change the crystallinity and electronic properties of the milled surface. The atomic collisions of 30 keV Ga ions with the lattice atoms create a 20-30 nm thick amorphous layer, while dopant deactivation extends up to at least 23 to 175 nm in highly and lowly doped regions, respectively.[72] The depth of these effects can be reduced by using lower beam energies, but it also depends on the ion beam element (e.g. Xe, Ne, Ar), impact angle, ion dose, and current density. Still, a change in the local resistivity of the material is inevitable, altering the SSRM resistance measurement and obstructing the straightforward conversion to active carrier concentration. Additionally, the introduction of three-dimensional architectures reduces the sampled material volume and adds multiple interfaces in the vicinity of the tip-sample contact. Interface traps create a depletion region, increasing the measured resistance. This effect is significant for highly doped regions thinner than 25 nm, with the onset of resistance increase occurring at even larger thicknesses in lowly doped regions. Furthermore, the tip-sample contact resistance starts to increase at film thicknesses below 10 nm due to the dependence of the β-Sn phase properties on the Si layer thickness and the elastic properties of the surrounding materials. Overall, many different phenomena influence SSRM measurements on confined volumes, and hence one needs to be careful in interpreting the SSRM data originating from state-of-the-art devices.

The repeatability (i.e. the ability to reproduce the measurement result using the same experimental conditions) of SSRM on silicon in air is typically better than 20% across the whole dynamic range, representing the deviation in the measured resistance along different line scans in a single measurement. The highest repeatability is achieved in

AIP Publishing Applied Physics Reviews ACCEPTED MANUSCRIPT
This is the author's peer reviewed, accepted manuscript. However, the online version of record will be different from this version once it has been copyedited and typeset.
PLEASE CITE THIS ARTICLE AS DOI: 10.1063/5.0280969

highly doped areas, explained by the more ohmic-like contact compared to lowly doped areas. The repeatability values can be further improved below 10% by measuring at a higher force or moving to argon, nitrogen or high vacuum environment. The improved performances under high vacuum are mainly linked to the removal of the water meniscus present in air which affects the pressure distribution in the underlying sample, reducing the force needed for the local β-Sn phase transition.[9] Therefore, also spatial resolution and tip lifetime are improved in vacuum conditions.[74]

The accuracy of conventional dopant quantification using SSRM was evaluated on medium-doped silicon (~1×10^{17} carriers/cm^3) to minimize the influence of tip resistance and surface states, thereby focusing on the intrinsic accuracy of the technique. Under these conditions, an accuracy of approximately 50% was achieved. Recent work proposed that the accuracy can be improved to 25% by bonding the sample of interest and the calibration standard face-to-face, ensuring identical cross-sectional polishing conditions and resulting surface morphology.[75] This approach eliminates preparation-induced deviations and allows for rapid tip movement, reducing the risk of tip degradation when transitioning from the region of interest (ROI) to the calibration sample. Further improvement to an accuracy of 20% can be achieved by incorporating additional calibration measurements, both before and after the analysis of the sample of interest, discarding measurements if the deviation is more than 1%. This ensures consistency in the calibration curve and confirms no tip degradation has occurred during the measurement process.

It is worth noting that recently the above-described SSRM data analysis workflow has been automated using artificial intelligence (AI)-based computer vision algorithms, as will be discussed in a later section of this review.[76] YOLO (You Only Look Once) models were trained to detect individual layers in SSRM resistance maps of a calibration sample to construct the calibration curve and subsequently convert resistance to carrier concentration maps for the sample of interest, significantly reducing the processing time. This example can be a steppingstone for automating more complex tasks, effectively addressing SSRM's throughput limitations on the data analysis side. Furthermore, automated data analysis could serve as feedback in a future AI-driven framework for

AIP Publishing Applied Physics Reviews ACCEPTED MANUSCRIPT
This is the author's peer reviewed, accepted manuscript. However, the online version of record will be different from this version once it has been copyedited and typeset.
PLEASE CITE THIS ARTICLE AS DOI: 10.1063/5.0280969

autonomous SSRM operation. The potential of AI for both data analysis and measurement automation applications has already been demonstrated in the broader SPM context in previous works.[77, 78]

SSRM the next decade

Areas of Development and Future Trends in SSRM

- Liquids environments

AFM in liquids is a well-established branch of nanoimaging with the sample and the probes submerged in a liquid environment. This method provides valuable information when studying materials and processes in their natural or near-natural state, for example, in electrochemical reactions, imaging cells, proteins, DNA, and other biomolecules in their native environment.[79] In most of these applications the imaging mode is non-contact or tapping where the cantilever oscillates near its resonance frequency, minimizing tip-sample interactions and reducing damage to soft samples. While counterintuitive for the analysis of inorganic materials, such as those reported in the review, SSRM performed in a liquid environment demonstrated multiple advantages and it represents an active area of research. Previous works reported on the use of oil as a suitable medium to overcome some of the issues associated with debris accumulation and the removal variability when working in air.[44] **Figure 10** shows the impact of oil on the readout scan of a crater region where scalpel SPM has been used to remove over 100 nm of material; the minimum presence of debris on the edges of the scan area is the net result of the use of oil. Other studies acquired with the same tip in air and oil attempted to compare the impact of the scanning environment on the formation and accumulation of debris.[44] The results confirm that the tip-induced removal is affected by the scanning environment, with a removal rate in oil approximately 2 to 4 times higher than in air, depending on the probe tip used.. In addition, the authors demonstrated that both environments yield good quality SSRM measurements, as visible from the clear appearance of all doping levels contained in the calibration structure. In our experiments the oil is collected by engaging the tip into a

AIP Publishing Applied Physics Reviews ACCEPTED MANUSCRIPT
This is the author's peer reviewed, accepted manuscript. However, the online version of record will be different from this version once it has been copyedited and typeset.
PLEASE CITE THIS ARTICLE AS DOI: 10.1063/5.0280969

larger droplet deposited close to a corner of the sample, acting as a reservoir, before moving to a fresh scan area (Figure 10c). This simple procedure allows the tip apex to retain enough oil at the tip-sample junction while minimizing any possible interference of the large oil droplet with the AFM laser. Castor bean oil having a higher viscosity compared to the usual inorganic mineral oil is selected which is less prone to evaporation from the tip.

Here, Figure 10d,e shows the acquisition of SSRM datasets for a nanosheet-FET and an array of Si Fins capped with Poly-Si (Figure 10e), as studied in an oil environment. Both images show no visible detrimental effects of the use of oil, with excellent spatial resolution (nm) with a single-digit dopant gradient (ca. 3nm/dec) and large dynamic range (10^{16} cm^{-3} to 10^{20} cm^{-3}). In Figure 10d, the measurement is acquired with a sharp diamond probe (Adama) and using 500 mV bias applied to the sample back-contact, with a resolution of ca. 2nm/pixel. Although the presence of the metal gate limited our resolution in the nanosheet channel regions, the presence of the two NS is clearly visible, thus suggesting how a dedicated test vehicle with a dummy gate could improve our resolution.

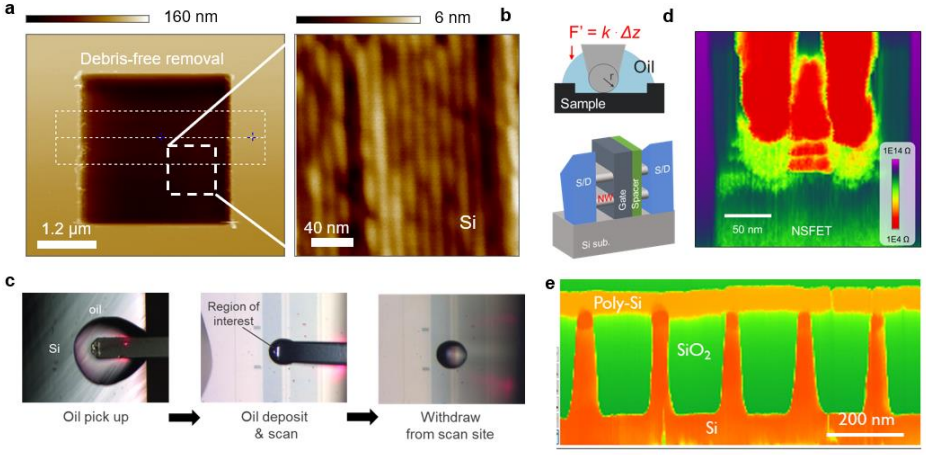

Figure 10: SSRM in liquid environment. **a**. AFM image showing debris-free removal of material using an oil-based technique. The left panel shows a larger area with a square

AIP Publishing Applied Physics Reviews ACCEPTED MANUSCRIPT
This is the author's peer reviewed, accepted manuscript. However, the online version of record will be different from this version once it has been copyedited and typeset.
PLEASE CITE THIS ARTICLE AS DOI: 10.1063/5.0280969

region where material has been removed. **b**. The right panel is a zoomed-in view of the removed region, revealing the underlying silicon (Si) machined surface. **c**. Optical microscopy images demonstrating the steps of the oil-based manipulation process: oil pick-up, oil deposit and scanning in the region of interest, and withdrawal. **d**. The schematic illustrates the principle of the oil-based SSRM and NSFET structure under test. **e**. Alternative data acquisition in the presence of different layers (Poly-Si, SiO_2, Si).

While these results clearly suggest a possible pathway for the feasibility of 3D tomographic SSRM studies in oil, the same analysis scheme could be used to favor mechanochemical reactions and eventually increase the interaction forces between the probe tip and the etched substrate. Therefore, beyond the suppression of debris formation, the use of oil in SSRM could be explored to improve control over the removal rate by offering an additional knob to increase (or reduce) the removal rate depending on the application. While this is not been reported yet for SSRM, it has been demonstrated by other groups by the presence of surface terminal species that locally modify the surface at the interface between the tip and the sample and affect the material removal rate.[80]

- Correlative metrology flow: in-situ SSRM with FIB-SEM-TEM

This fusion of technologies provides a synergistic platform for advanced characterization, particularly valuable in the context of CMOS process development and failure analysis, where understanding the interplay between nanoscale structure and electrical functionality is paramount. In-situ analytical flows with SSRM refer to measurement techniques that are co-integrated within the same instrument and they represent a significant advancement in nanoscale characterization of advanced CMOS. FIB-SEM's precise cross-sectioning and high-resolution imaging capabilities, when coupled with SSRM's ability to map carrier concentration, offer a powerful means to understand the complex interplay between device structure and electrical performance. This approach is particularly crucial for analyzing modern semiconductor devices where three-dimensional architectures and intricate doping profiles dictate the device

AIP Publishing Applied Physics Reviews ACCEPTED MANUSCRIPT
This is the author's peer reviewed, accepted manuscript. However, the online version of record will be different from this version once it has been copyedited and typeset.
PLEASE CITE THIS ARTICLE AS DOI: 10.1063/5.0280969

functionality. Moreover, with ultra-scaled devices, the accurate landing of the AFM probe can preserve the tip-apex quality, thus allowing for the highest obtainable resolution in the case of electrical AFM modes. This concept often comes to the rescue of complex problems in which one individual technique is simply not enough. The combination of SSRM with FIB-SEM is particularly effective as it allows for real-time monitoring and control of critical parameters without the need to remove the sample or interrupt the analysis.

The process flow can be implemented with a dedicated sample preparation that shares many of the conventional aspects of FIB-induced TEM lamella preparation (**Figure 11**). The area of interest can be extracted, and the conventional TEM grid serves as a carrier for the sample (Figure 11a). The first attempts used relatively thick lamellas without any additional electrical connection, resulting in poor electrical back-contact and high series resistance (Figure 11b). However, the procedure has been refined, with the thinning of the area of interest and the addition of e-beam deposited W or Pt to anchor the lamella, while improving the electrical back-contact (Figure 11a right). This improved sample preparation enabled the execution of correlative metrology flows where SSRM could be combined with TEM in the exact same areas.

This is obtained by adding a small FIB-induced slit under the sample, thus enabling electron transmission in the area of interest. To date, the lack of a fully integrated system with TEM and AFM in a single tool requires for the analysis to be interrupted and the sample to be transferred between multiple instruments. While adding time to the final analysis, this implementation can still be rewarding due to the higher level of information accessible from correlating multiple readouts. This class of in-situ metrology workflows, such as combining SSRM, FIB-SEM, and EDX, provides a powerful approach for comprehensive device characterization. Figure 11c shows the case of a FinFET, where the corresponding high-angle annular dark-field scanning transmission electron microscopy (HAADF-STEM) reveals the layered structure, featuring boron-doped silicon germanium (B-doped SiGe) S/D in a germanium Fin, complemented by SSRM and energy dispersive X-ray spectroscopy (EDX) maps. Figure 11d demonstrates the use of the same method to identify and reconstruct, in 3D with scalpel SPM, a misprocessed Si

Applied Physics Reviews ACCEPTED MANUSCRIPT
This is the author's peer reviewed, accepted manuscript. However, the online version of record will be different from this version once it has been copyedited and typeset.
PLEASE CITE THIS ARTICLE AS DOI: 10.1063/5.0280969
AIP Publishing

Fin, while Figure 11e shows the analysis flow applied to investigate the impact of thermal annealing for the curing defects at the top surface of a Si Fin.[81]

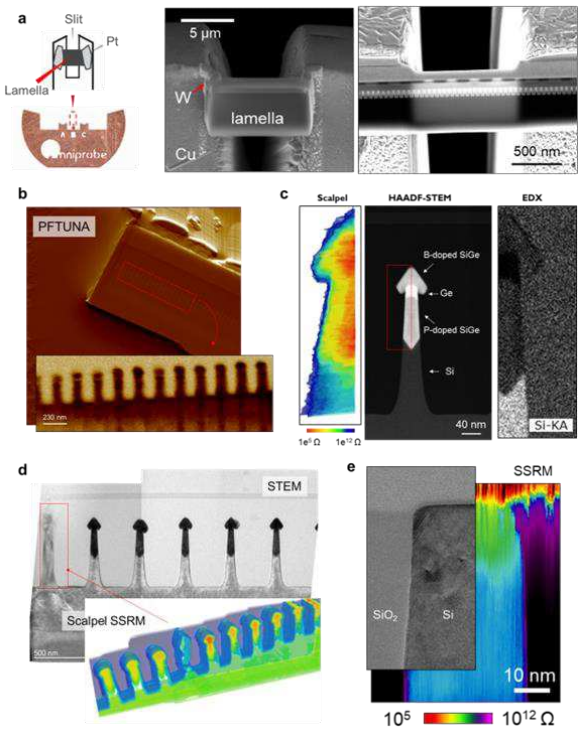

Figure 11: Correlative metrology flow: in-situ SSRM with FIB-SEM-TEM. **a**. Schematic of the customized TEM grid used for the correlative metrology flow. Comparing a thick sample (i.e., lamella) and an electron transparent sample. **b**. The role of high series resistance in thick lamellas influences the lateral resolution and sharp contrast. **c**. The use of thin lamellas mitigates the problems by adding the possibility to correlate SSRM with STEM and EDX. **d**. Demonstration of scalpel SSRM performed on a lamella sample. Here, the 3D reconstruction is limited by the reduced thickness of the lamella. **e**. Comparison of TEM and SSRM for the estimation of surface defect recovery and their impact on Fin doping activation.

AIP Publishing Applied Physics Reviews ACCEPTED MANUSCRIPT
This is the author's peer reviewed, accepted manuscript. However, the online version of record will be different from this version once it has been copyedited and typeset.
PLEASE CITE THIS ARTICLE AS DOI: 10.1063/5.0280969

Originally developed as a custom solution for highly complex devices, this workflow is now widely adopted in failure analysis labs. Its complementary nature is evident when considering the strengths of each technique: FIB-SEM provides high-resolution 3D tomographic reconstructions of the volume of interest, SSRM encodes the electrical resistance of interconnects and enables carrier profiling of source/drain regions and the channel, and EDX offers compositional analysis. This comprehensive approach, integrating structural and electrical characterization within a single, streamlined workflow, offers a significant advantage in understanding the intricate properties of semiconductor devices. The convergence of these complementary techniques provides a holistic view of device performance, enabling researchers and engineers to correlate physical structures with electrical behavior, leading to more effective process development and failure analysis. This approach leverages the synergies of each technique to gain a deeper understanding of device characteristics, particularly in ultra-confined volumes. It is worth noting that the advent of modern dual beam systems with laser and plasma FIB, where various gases such as Xe, Ar, and oxygen are used for the ion milling, is paving the way for broader adoption of these strategies, offering potential improvements in SSRM quality, faster sample preparation, and recovery of resolution and quantitative analysis.

Similarly, it is important to mention that while TEM and AFM remain separated instruments, the scientific community has witnessed a surge in the development of hybrid microscopes in recent years. Recognizing the power of this integrated approach, the last decades have seen the wide integration of self-sensing and optically detected AFM modules inside FIB-SEM instruments. These innovative tools combine the capabilities of conventional electron beam techniques, such as SEM, EDX, and FIB, with the high-resolution electrical mapping of SPM, exemplified by SSRM. However, as highlighted in this review, the quality of an SSRM measurement ultimately relies on abalanced combination ofoptimal surface preparation, and well-controlled tip-sample junction pressure. In the area of self-sensing AFM, electrical modes still lag behind in terms of

AIP Publishing Applied Physics Reviews ACCEPTED MANUSCRIPT
This is the author's peer reviewed, accepted manuscript. However, the online version of record will be different from this version once it has been copyedited and typeset.
PLEASE CITE THIS ARTICLE AS DOI: 10.1063/5.0280969

pressure control, and high-performance tip coatings. By addressing these points, the use cases for CMOS failure analysis can rapidly multiply.

- Multi-probe analysis schemes

a. RPM-3D

In the section on scalpel SSRM the ability of tomographic SSRM imaging obtained by a slice-and-view approach has been introduced. However, some of the considerations on the tip-induced removal rate, and its estimation are an oversimplification of the original problem. For example, a more realistic view of the pressure-induced removal scenario for the case of FinFET is reported in Supporting Information Figure S2. Here, the presence of multiple materials suggests that slight variations in their threshold for plastic deformation will induce local variations of the removal rate. For example, faster erosion for areas containing metals, such as the gate, compared to areas containing SiO_2. This effect, although measurable through the AFM morphology channel, is generally not considered in the extraction of the removal rate. Accounting for it could improve the implementation of scalpel SSRM if for example, the local morphology contained in the AFM would be used to modulate the tip-sample pressure on a pixel-by-pixel base, or by exploring a double-pass solution. Moreover, in case of accessing deep structures or features buried under multiple metallization layers, it is not convenient to use the same probe for probing and removing, as it would result in poor resolution due to a damaged probe.

Applied Physics Reviews ACCEPTED MANUSCRIPT
AIP Publishing
This is the author's peer reviewed, accepted manuscript. However, the online version of record will be different from this version once it has been copyedited and typeset.
PLEASE CITE THIS ARTICLE AS DOI: 10.1063/5.0280969

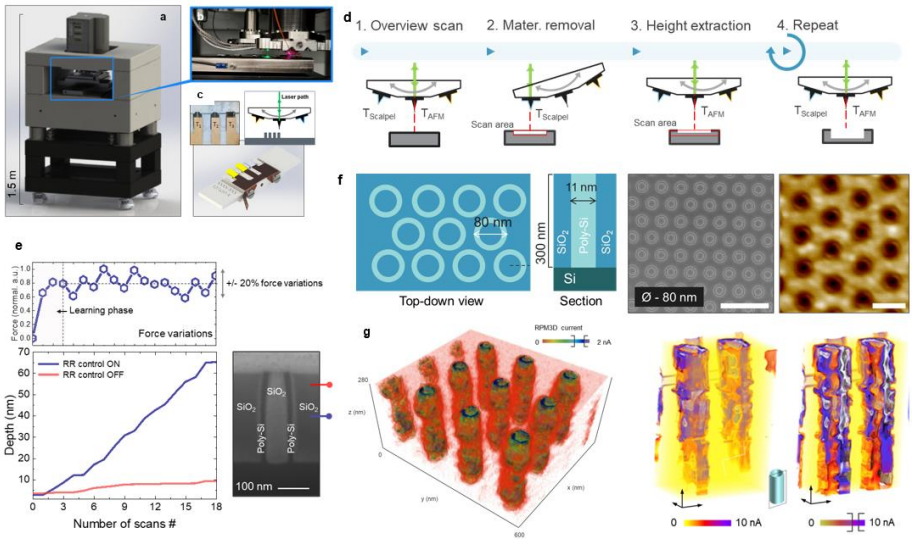

Figure 12: **a**. 3D rendering of the RPM-3D system. The blue rectangle indicates the region magnified in panel **b**. A close-up photograph reveals the sample stage within the RPM-3D system and the tiltable scan head. **c**. Detailed view of the sample holder with multiple probes. **d**. Schematic representation of the multi-probe removal and sensing analysis flow in the RPM3D. **e**. Comparison of depth removal w/o RR control for a 3D NAND dummy structure, in the inset. Note that the top inset shows the continuous adjustments of the load force during removal for the case of RR control ON. **f**. 2D schematics of the 3D NAND dummy structure, supported by TEM and AFM images of the sample. **g**. Reconstructed 3D tomographic view of the volume under study, with detailed view of a single vertical channel.

To mitigate these situations, while improving removal rate control, a multi-probe system design separating the scalpel and sensing responsibilities has been explored.[82] A standalone microscope named Rapid Probe Microscope (RPM-3D) implements this feature through the addition of a tiltable axis to the scanner, allowing for the rapid interchange between up to 3 different, and customizable probe tips. The RPM-3D has a custom-built insulating clip cassette, that allows for the interchange between probe types,

AIP Publishing Applied Physics Reviews ACCEPTED MANUSCRIPT
This is the author's peer reviewed, accepted manuscript. However, the online version of record will be different from this version once it has been copyedited and typeset.
PLEASE CITE THIS ARTICLE AS DOI: 10.1063/5.0280969

ensuring that the optimized probe tip is used for each tier of a slice and sense tomographic data set (Figure 12). Paired with the self-adjusting capability of the removal rate by dynamically varying load force, each scan improves the quality and speed of data acquisition, supports automation, enables high-dimensional data handling, and extends volumetric sensitivity (range 10^7-10^{12} nm^3), thereby offering volumetric mapping of electrical properties in the area of interest, including SSRM. A detailed description of the RPM-3D operations is reported elsewhere.[47, 82]

b. Reverse Tip Sample (RTS) SSRM

Recently, yet another promising multi-tip approach has emerged, known as reverse tip sample (RTS) SPM. The core idea is to reverse the traditional AFM tip-sample arrangement to overcome the above-discussed challenges, without the need for new multi-tip AFM instruments or any hardware modifications to the existing single-tip ones. In the RTS configuration, the sample is mounted on a tipless cantilever, while the tips are integrated into a nanofabricated RTS probe chip which takes the sample's place. This results in a straightforward concept that provides all the multi-tip benefits. Indeed, and again in the context of electrical tomography, multiple tips can be used for successive scans, each assigned distinct roles such as material removal, imaging, and current sensing. Furthermore, since the RTS probe chip contains thousands of tips, entire groups can now be allocated to a single task, significantly boosting the statistical confidence of the measurements. However, having an abundance of tips is only one part that makes this possible, another is the capability to seamlessly switch between them. In the RTS configuration, exchanging tips is simply done by applying piezo or coarse motor XY offsets that match the tip-to-tip spacing on the RTS probe chip to reposition the cantilever holding the sample to the next neighboring tip, allowing the scanning to resume in the same region of interest within seconds and without disrupting the experiment. Kim et al.[83] laid the groundwork for RTS SPM technology by developing a nanofabrication protocol for bare Si RTS probe chips. This process, based on inductively coupled plasma reactive ion etching (ICP-RIE), utilizes multiple alternating anisotropic and isotropic etching steps of p-type〈100〉Si wafers. They also further demonstrated the functionalization of these

Applied Physics Reviews ACCEPTED MANUSCRIPT
This is the author's peer reviewed, accepted manuscript. However, the online version of record will be different from this version once it has been copyedited and typeset.
PLEASE CITE THIS ARTICLE AS DOI: 10.1063/5.0280969
AIP Publishing

Si probe chips with conductive coatings, including platinum (Pt) and more importantly for SSRM, boron-doped diamond (BDD). A comprehensive description of the nanofabrication process is provided in the original article.

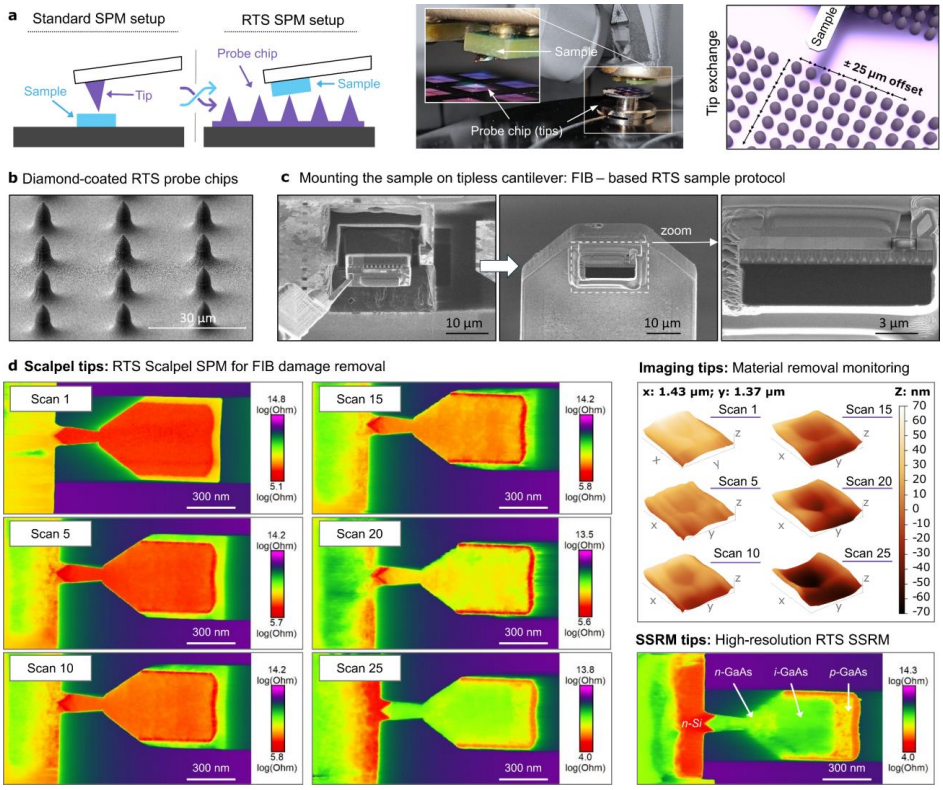

Figure 13: a. RTS SPM concept: schematic comparison of the standard and RTS configurations, a photograph of a conventional AFM instrument that is set up for RTS measurements, and a 3D representation of the tip layout and exchange process in RTS SPM. **b**. SEM image of a boron-doped diamond (BDD) – coated Si RTS probe chip. **c**. SEM images illustrating the FIB-based RTS sample preparation procedure, in which GaAs nanoridge laser diode structures are mounted onto a tipless cantilever. **d**. RTS SSRM measurement results obtained from the same sample, presenting SSRM images

AIP Publishing Applied Physics Reviews ACCEPTED MANUSCRIPT
This is the author's peer reviewed, accepted manuscript. However, the online version of record will be different from this version once it has been copyedited and typeset.
PLEASE CITE THIS ARTICLE AS DOI: 10.1063/5.0280969

captured at different stages of FIB-damaged material removal. Also shown are topography images of the surface at the same points of the removal process, as well as an SSRM image of the exposed nanostructure acquired using a separate, unused tip on the BDD-coated RTS probe chip.

Following these developments, the RTS sample preparation became the next critical element for RTS SSRM. Lagrain et al[84], established FIB protocols to mount both top-view and cross-sectional samples onto the tipless cantilever. A different example of the latter is shown in Figure 13c, where a GaAs nanoridge laser diode structures, previously discussed and presented in Figure 8 in the context of standard SSRM measurements, is now mounted on the tipless cantilever. This study also marked the first demonstration of SSRM measurements being done in the RTS configuration using multi-wall carbon nanotube (MWCNT) interconnects (top-view) and memory-hole samples (cross-section). Although these experiments produced qualitative results, they confirmed the viability of the RTS configuration for SSRM. The qualitative nature of the data was primarily due to unavoidable FIB-induced damage during sample preparation. This limitation could potentially be addressed in the future through the development of improved sample preparation methodologies. In the meantime, FIB-induced damage can be mitigated by removing the affected layers using Scalpel SPM. This is where the multi-tip functionality of the RTS configuration can be fully exploited. Returning to the GaAs nanoridges shown in panel c, for which RTS SSRM measurements are now presented in panel d, designated "scalpel tips" can be used to remove the FIB-damaged layers, while the process is monitored using separate "imaging tips." Once the buried, undamaged region of the nanostructure is exposed, any number of fresh, sharp tips can then be used to perform RTS SSRM to acquire high-resolution resistance maps. While it is true that RTS technology is still in development and has yet to reach its full potential for SSRM, another recent piece of work has highlighted the benefits of its early adoption to drive AI applications in SSRM, which will be considered as part of the broader discussion in the next section.

AIP Publishing Applied Physics Reviews ACCEPTED MANUSCRIPT
This is the author's peer reviewed, accepted manuscript. However, the online version of record will be different from this version once it has been copyedited and typeset.
PLEASE CITE THIS ARTICLE AS DOI: 10.1063/5.0280969

c. Artificial intelligence (AI) for SSRM

In recent years, the use of artificial intelligence (AI), including machine learning (ML) and deep learning (DL), has increased significantly across many scientific and technological domains, and the SPM field is no exception. In the context of SPM, ML algorithms can be trained to identify patterns and relationships directly from raw spectroscopic data, while DL methods, particularly convolutional neural networks (CNNs), are especially effective at interpreting complex, image-centered datasets. For example, AI-based workflows have been developed for autonomous SPM operation, specific region selection, image quality assessment, and probe conditioning.[78] On the analysis side, AI has also been applied to a broad range of tasks, including classification, localization, and segmentation of various image features, as well as denoising, reduction of measurement uncertainty, prediction of physical properties, etc. A comprehensive overview of recent developments, challenges, and future directions in the implementation of AI in SPM is provided by Laskar et al.[68]

Although many of these applications clearly demonstrate the potential of AI in the field, its broader adoption still remains rather limited due to the inherently low throughput of SPM techniques, which leads to a lack of large, high-quality datasets needed for effective model training. This is especially true for SSRM, where reduced throughput stems from the high-force operational regime of the technique. The elevated contact pressures accelerate tip wear and increase the risk of tip breakage, requiring frequent tip replacements. In fact, during the measurements, one needs to maintain a delicate balance between applying enough force to induce the β-tin phase transition for doping contrast while avoiding excessive force that will degrade the spatial resolution and/or damage the tip. This data collection complexity is not only making it difficult to compile large enough training datasets needed for the AI model training but also hinders the development and deployment of AI-driven automation to make it more efficient. In other words, a cycle emerges in which limited data availability hinders AI implementation, while the lack of AI-driven data collection further contributes to insufficient data for effective model training. Nevertheless, there have been some pioneering efforts for data analysis indicating early progress and potential for future developments.

AIP Publishing Applied Physics Reviews ACCEPTED MANUSCRIPT
This is the author's peer reviewed, accepted manuscript. However, the online version of record will be different from this version once it has been copyedited and typeset.
PLEASE CITE THIS ARTICLE AS DOI: 10.1063/5.0280969

On the ML front, recent work focused on the development of a tool called MultiDAT-AFM to process and analyze hyperspectral data from AFM DataCube modes, demonstrating the successful integration of supervised machine learning algorithms to predict 2D resistance maps as a function of bias voltage in DCUBE-SSRM.[67] Among the models tested, a refined Random Forest Regressor (RFR-R) achieved high predictive accuracy (R^2 = 0.90, RMSE = 0.18) when benchmarked against the experimental data. Indeed, the comparisons between predicted and measured 2D resistance maps at multiple DC bias values confirmed the model's ability to replicate spatial variations in electrical behavior. In addition to improving the data analysis, this work also illustrates well the potential of applying AI to SSRM, as predictive models such as these can help accelerate the data collection by reducing the need for extensive physical measurements, with predicted maps effectively complementing the experimental ones.

Moving on to deep learning, the data processing workflow in quantitative SSRM presented a clear opportunity for automation. As discussed earlier in this review, once resistance maps are obtained from both the target sample and a calibration sample with known doping levels using identical measurement conditions and the same probe, the subsequent data processing is relatively straightforward but highly inefficient in practice. Each calibration takes around 15 minutes and requires the use of three separate software tools, along with tedious manual annotation of each resistance layer in the calibration sample's SSRM map. This workflow does not scale well with large datasets, which is particularly problematic given that multiple calibrations are typically required for a single sample analysis. Interestingly, the standardized and repetitive nature of the calibration procedure makes it well-suited for AI implementation, as sufficiently large training datasets are available. Wouters et al. explored an AI-based computer vision approach that automates the entire calibration procedure.[66] An overview of the development process described in this work is illustrated in Figure 14. Convolutional neural network-based AI models (specifically YOLOv5) were trained to identify individual doping layers in the SSRM resistance map of the calibration sample, while avoiding measurement artifacts (Figure 14a). The training dataset comprised 80 SSRM images acquired from measurements on calibration samples using roughly 30 different tips (Figure 14b). Custom image augmentation techniques were used to expand the dataset to 480 images,

AIP Publishing Applied Physics Reviews ACCEPTED MANUSCRIPT
This is the author's peer reviewed, accepted manuscript. However, the online version of record will be different from this version once it has been copyedited and typeset.
PLEASE CITE THIS ARTICLE AS DOI: 10.1063/5.0280969

enabling more effective and robust model training (Figure 14c). Model evaluation with fixed custom test datasets ensured consistent performance metrics (accuracy, precision, recall) and fair comparisons between models. The testing results demonstrated a high model performance in detecting and identifying doping layers, with accuracy values of 98.3% and 99.4% for models trained on datasets without and with augmentation, respectively (Figure 14d). This accurate layer detection enabled the automation of subsequent data processing steps, including resistance extraction for each layer (R1, R2, R3 etc.), calibration curve construction, and conversion of resistance maps to carrier concentration maps of the sample of interest, thereby successfully automating the whole quantitative SSRM data processing workflow.

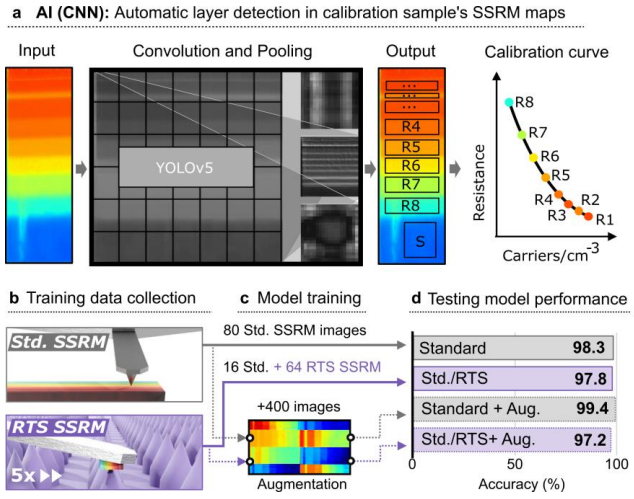

Figure 14: Automating quantitative SSRM data analysis with an AI computer vision-based approach and supported by RTS SSRM measurements, presented through the development process, which includes **a**. defining platform functionality, **b**. building training datasets from standard and RTS SSRM measurements, **c**. model training and **d**. performance testing of the resulting AI models.

Importantly, this study also explored the potential of using emerging high-throughput SPM technologies, such as RTS SPM (described earlier), to significantly accelerate the generation of AI training datasets for more specialized and less routine SSRM workflows

AIP Publishing Applied Physics Reviews ACCEPTED MANUSCRIPT
This is the author's peer reviewed, accepted manuscript. However, the online version of record will be different from this version once it has been copyedited and typeset.
PLEASE CITE THIS ARTICLE AS DOI: 10.1063/5.0280969

where large datasets are not readily available. However, this strategy would only be viable if AI models trained on these datasets would perform comparably to those trained on data generated using the standard SSRM configuration. As a proof-of-concept, a dedicated training dataset was created, consisting of 16 images (20%) from standard SSRM and 64 images (80%) from RTS SSRM, resulting in a fivefold reduction in total data collection time for the same number of tips being used (Figure 14b,c). Subsequent testing revealed that incorporating RTS data had no significant impact on model performance, yielding accuracy values of 97.8% and 97.2% without and with augmentation, respectively (Figure 14d).

As the first demonstrations of AI applied to SSRM, these examples lay essential groundwork for future efforts to automate even more complex tasks, directly addressing throughput limitations in both data collection and analysis, as it has already been largely demonstrated in the broader SPM context.

Probes Technology Development

The importance of probe technology in SSRM has been introduced since the first section of this review. By providing a side-by-side comparison between the SSRM results and the enabling probe technology, Figure 1 shows the critical role of conductive probes engineering over the course of the years. The deep relationship between probes and obtainable results has been based on the steady innovations and improvements in the fabrication of conductive diamond tips in the last 30 years and continues to these days. Boron-doped diamond was from the start the tip material of choice and the lack of suitable microfabrication technologies for diamond tips was a major challenge for SSRM in its infant days. The first probes used for demonstrating the SSRM principle were composed of sharpened diamond crystals (with ~100 nm tip radius) implanted with boron, which were manually attached to metal wires acting as a cantilever beam structure (**Figure 15**a).[85] The first micromachined diamond probes were Si probes coated with a thin diamond layer[86]; these are referred to as coated diamond tip (CDT) probes (Figure 15b). With these probes, the first high-resolution two-dimensional (2D) SSRM measurements of planar transistor structures were demonstrated. Such CDT probes are still being used

AIP Publishing Applied Physics Reviews ACCEPTED MANUSCRIPT
This is the author's peer reviewed, accepted manuscript. However, the online version of record will be different from this version once it has been copyedited and typeset.
PLEASE CITE THIS ARTICLE AS DOI: 10.1063/5.0280969

today but they suffer from two problems: multiple-tip images are often observed – they originate from the presence of several diamond nanocrystals at the apex region which make electrical contact to the region of interest at the same time; and CDT's are often breaking close to the apex region while being scanned at ~8-12 GPa pressure. Therefore, pyramidal diamond tips - commonly referred to as full diamond tips (FDT) - have been developed (Figure 15c) [86] [87] [88]. Their diamond body and low aspect ratio gives them very high mechanical stability. They are made by the molding technique, resulting in a smaller tip radius compared to CDTs. This allows us to routinely perform SSRM measurements with nanometer spatial resolution and has also opened the door for carrying out the first 3D SSRM measurements.[89] Despite these advancements, the increased materials complexity in combination with confined volumes in sub-10 nm technology nodes led to typical materials smearing artifacts in SSRM measurements when using such low-aspect-ratio FDTs. Therefore, in the next phase, nanoscopic diamond tips with a higher aspect ratio and ultra-high sharpness, placed on top of a pedestal tip support structure, were developed (Figure 15d)[90] and have, in recent years, become the preferred probe tip configuration for measuring the most advanced nanoelectronics device structures by SSRM. Note that other interesting diamond tip concepts have also been developed and prototyped over the years, like in-plane diamond tips[91], overcoated diamond tips (ODT)[92], and hedgehog full diamond tips (HFDT).[93] A summary table listing the fabrication method, tip sharpness, and main applications of these different types of diamond tips was provided by Wouters et al.[82]

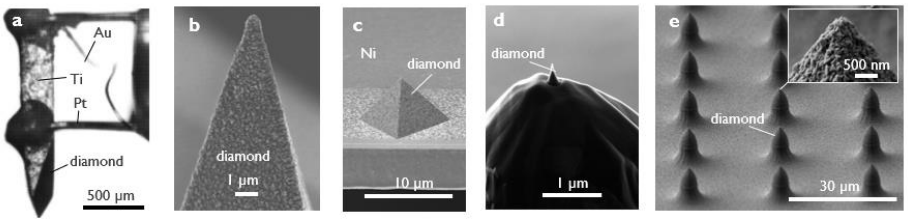

Figure 15: SSRM diamond probes: **a**. Handmade diamond probe, **b**. coated diamond tip (CDT), **c**. full diamond tip (FDT), **d**. nanoscopic diamond tip, **e**. diamond tip array for reverse tip sample (RTS) configuration.

AIP Publishing Applied Physics Reviews ACCEPTED MANUSCRIPT
This is the author's peer reviewed, accepted manuscript. However, the online version of record will be different from this version once it has been copyedited and typeset.
PLEASE CITE THIS ARTICLE AS DOI: 10.1063/5.0280969

Besides these probe manufacturing aspects, continuous advances in the diamond thin-film deposition knowhow and its fundamental understanding over the past three decades were equally important to achieve high-performance diamond tips. The establishment of optimized nanodiamond seeding procedures for tip applications has proved key to grow ≥100 nm thick closed diamond layers by chemical vapor deposition (CVD).[94] The development of the hot-filament CVD (HFCVD) method should be mentioned, which allows today to deposit thin nanocrystalline and microcrystalline boron-doped diamond coatings with a high uniformity over large wafer substrates.[94] The conductivity of NCD and MCD films was optimized to achieve as high as possible layer conductivity (~5 mΩ/cm) while being wear-resistant at the same time. In comparative studies, MCD films performed clearly better than NCD films and were therefore used as standard films for SSRM tips.[95]

Today, the highest performing boron-doped diamond tips allow us to routinely measure the carrier profile with a spatial resolution of ≤1 nm. These super-sharp tips are, however, rapidly blunting because of the involved scanning at extreme pressures of 8-12 GPa. The resulting short tip lifetime is therefore currently the biggest hurdle for further advances, especially in the area of 3D SSRM measurements. Frequent manual probe changes are not an effective solution because they are time-consuming (~10 min/tip), cumbersome (ROI must be relocated after each probe change), and expensive (typically >$100/tip). Effective solutions to cope with this could be multiple-probe systems (e.g. probe switching enabled by rotating multiple-probe holder)[47] and automatic probe exchangers (as commonly used already for in-line SPM tools). Another promising path currently being explored is reverse tip sample SPM, introduced in detail in the previous section, which employs tip chip arrays with hundreds to thousands of individual sharp diamond tips (Figure 15e)[73] that can be switched within seconds.[96]

Conclusions:

This review has traced the development of scanning spreading resistance microscopy over the past thirty years, emphasizing the key challenges that have shaped its evolution. A central theme has been the close and crucial relationship between SSRM and the

AIP Publishing Applied Physics Reviews ACCEPTED MANUSCRIPT
This is the author's peer reviewed, accepted manuscript. However, the online version of record will be different from this version once it has been copyedited and typeset.
PLEASE CITE THIS ARTICLE AS DOI: 10.1063/5.0280969

progress of CMOS logic device fabrication, illustrating how the technique has consistently adapted to meet the demands of new device architectures.

As the nanoelectronics industry progresses beyond traditional miniaturization, the focus is shifting towards more complex three-dimensional nanostructures and the heterogeneous integration of diverse materials. In this landscape, physical characterization and metrology must be tailored to specific processes, materials, and device parameters to maintain their effectiveness. SSRM has demonstrated a strong capacity for innovation, consistently delivering high-precision electrical property analysis and expanding its capabilities to three-dimensional measurements. Even today, it provides an excellent platform for obtaining comprehensive information about the electrical characteristics of devices under test. SSRM, with its ability to probe electrical properties at the nanometer scale, has become a vital component of integrated metrology strategies. By directly measuring parameters like carrier concentration and resistivity, SSRM offers crucial insights into the electrical behavior of devices, complementing the structural and compositional data provided by techniques such as SEM, FIB, and EDX. This combination of information enables researchers to effectively identify and analyze critical features—including doping profiles, interconnect resistance, and defect-related electrical variations—ultimately driving more efficient process optimization and more effective failure analysis.

However, like many analytical techniques, SSRM faces emerging challenges related to the fundamental physics of sensing at ultra-confined volumes and in face of ever more complex 3D logic devices. With an increasing complexity of application-specific architectures, SSRM has proven a solid record of innovation to probe matter, delivering high precision, expanding in 3D, and still, nowadays, offering an excellent platform to gain a complete set of information about the electrical properties of the device under test. For process integration issues such as variability reduction, precise control of threshold voltages, junction placement, doping profiles, and leakage current suppression, the semiconductor metrology community is actively pursuing novel solutions and exploring new physical principles to address these measurement gaps. This review focuses on some of the most promising pathways to continue applying SSRM, including the use of

AIP Publishing Applied Physics Reviews ACCEPTED MANUSCRIPT
This is the author's peer reviewed, accepted manuscript. However, the online version of record will be different from this version once it has been copyedited and typeset.
PLEASE CITE THIS ARTICLE AS DOI: 10.1063/5.0280969

multi-probes sensing, liquid environments, novel probe architectures and AI-based data analysis schemes. These are considered as some of the possibilities that the technique will embrace to continue providing value to the semiconductor industry in the next decade.

Supplementary Material

In the supplementary material we report on the impact of high-pressure scan and how it can induce a crater in the SSRM area of interest, SSRM resistance profile as a function of lateral distance across the FinFET structure, Scalpel SSRM 2D resistance profiles at low contact force for the NSFET, SSRM resistance measurement of a p-type doped silicon staircase calibration sample etc.

Acknowledgement

A.P. acknowledges FWO for the Strategic Basic Research PhD fellowship grant 1S20225N. The authors extend their sincere gratitude to Prof. Wilfried Vandervorst, a pioneer in this field, whose foundational work and continued influence have impacted all aspects of this work directly and indirectly to this day.

References

(1) Chau, R.; Doyle, B.; Datta, S.; Kavalieros, J.; Zhang, K.; Chau, R.; Doyle, B.; Datta, S.; Kavalieros, J.; Zhang, K. Integrated nanoelectronics for the future. *Nature Materials 2007 6:11* **2007/11**, *6* (11). DOI: 10.1038/nmat2014.
(2) Clarysse, T.; Eyben, P.; Parmentier, B.; Van Daele, B.; Satta, A.; Vandervorst, W.; Lin, R.; Petersen, D. H.; Nielsen, P. F. Advanced carrier depth profiling on Si and Ge with micro four-point probe. *Journal of Vacuum Science & Technology B: Microelectronics and Nanometer Structures Processing, Measurement, and Phenomena* **2008/01/01**, *26* (1). DOI: 10.1116/1.2802101.
(3) Clarysse, T.; Vandervorst, W.; Lin, R.; Petersen, D. H.; Nielsen, P. F. Beyond SRP: Quantitative carrier profiling with M4PP. *Nuclear Instruments and Methods in Physics Research Section B: Beam Interactions with Materials and Atoms* **2006/12/01**, *253* (1-2). DOI: 10.1016/j.nimb.2006.10.049.
(4) Clarysse, T.; Caymax, M.; Vandervorst, W. Impact of three-dimensional lateral current flow on ultrashallow spreading resistance profiles. *Applied Physics Letters* **2002/04/01**, *80* (13). DOI: 10.1063/1.1464224.
(5) Binnig, G.; Rohrer, H. Scanning tunneling microscopy---from birth to adolescence. *Reviews of Modern Physics* **1987-07-01**, *59* (3). DOI: 10.1103/RevModPhys.59.615.

AIP Publishing Applied Physics Reviews ACCEPTED MANUSCRIPT
This is the author's peer reviewed, accepted manuscript. However, the online version of record will be different from this version once it has been copyedited and typeset.
PLEASE CITE THIS ARTICLE AS DOI: 10.1063/5.0280969

(6) Binnig, G.; Quate, C. F.; Gerber, C. Atomic Force Microscope. *Physical Review Letters* **1986**, *56* (9), 930-933. DOI: 10.1103/PhysRevLett.56.930.
(7) Meyer, G.; Amer, N. M. Novel optical approach to atomic force microscopy. *Applied Physics Letters* **1988**, *53* (12), 1045-1045. DOI: 10.1063/1.100061.
(8) Bian, K.; Gerber, C.; Heinrich, A. J.; Müller, D. J.; Scheuring, S.; Jiang, Y.; Bian, K.; Gerber, C.; Heinrich, A. J.; Müller, D. J.; et al. Scanning probe microscopy. *Nature Reviews Methods Primers 2021 1:1* **2021-05-13**, *1* (1). DOI: 10.1038/s43586-021-00033-2.
(9) Eyben, P.; Mody, J.; Vemula, S. C.; Vandervorst, W. Impact of the environmental conditions on the electrical characteristics of scanning spreading resistance microscopy. *Journal of Vacuum Science & Technology B: Microelectronics and Nanometer Structures Processing, Measurement, and Phenomena* **2008/01/01**, *26* (1). DOI: 10.1116/1.2805250.
(10) Murrell, M. P.; Welland, M. E.; O'Shea, S. J.; Wong, T. M. H.; Barnes, J. R.; McKinnon, A. W.; Heyns, M.; Verhaverbeke, S. Spatially resolved electrical measurements of SiO2 gate oxides using atomic force microscopy. *Appl. Phys. Lett.* **1993**, *62*, 786-786.
(11) Shea, S. J. O.; Atta, R. M.; Murrell, M. P.; Welland, M. E.; Shea, S. J. O.; Atta, R. M.; Murrell, M. P.; Welland, M. E. Conducting atomic force microscopy study of silicon dioxide breakdown Conducting atomic force microscopy study of silicon dioxide breakdown. **2014**, *1945* (1995). DOI: 10.1116/1.588113.
(12) Matey, J. R.; Blanc, J. Scanning capacitance microscopy. *Journal of Applied Physics* **1985**, *57* (5), 1437-1444. DOI: 10.1063/1.334506.
(13) W. Vandervorst, M. Meuris, Method for resistance measurements on a semiconductor element with controlled probe pressure. 5369372 (1994).
(14) De Wolf, P.; Snauwaert, J.; Clarysse, T.; Vandervorst, W.; Hellemans, L. Characterization of a point-contact on silicon using force microscopy-supported resistance measurements. *Applied Physics Letters* **1995**, *66* (12), 1530-1530. DOI: 10.1063/1.113636.
(15) De Wolf, P. Cross-sectional nano-spreading resistance profiling. *Journal of Vacuum Science & Technology B: Microelectronics and Nanometer Structures* **1998**, *16* (1), 355-355. DOI: 10.1116/1.589810.
(16) Vandervorst, W.; Meuris, M. Method for resistance measurements on a semiconductor element with controlled probe pressure. Google Patents: 1994.
(17) Clarke, D. R.; Kroll, M. C.; Kirchner, P. D.; Cook, R. F.; Hockey, B. J. Amorphization and Conductivity of Silicon and Germanium Induced by Indentation. *Physical Review Letters* **1988-05-23**, *60* (21). DOI: 10.1103/PhysRevLett.60.2156.
(18) Hu, J. Z.; Merkle, L. D.; Menoni, C. S.; Spain, I. L. Crystal data for high-pressure phases of silicon. *Physical Review B* **1986**, *34* (7), 4679.
(19) Pharr, G.; Oliver, W.; Cook, R.; Kirchner, P.; Kroll, M.; Dinger, T.; Clarke, D. Electrical resistance of metallic contacts on silicon and germanium during indentation. *Journal of materials research* **1992**, *7* (4), 961-972.
(20) Mylvaganam, K.; Zhang, L. C.; Eyben, P.; Mody, J.; Vandervorst, W. Evolution of metastable phases in silicon during nanoindentation: mechanism analysis and experimental verification. *Nanotechnology* **2009**, *20* (30), 305705-305705. DOI: 10.1088/0957-4484/20/30/305705.
(21) Zhang, L.; Tanimoto, H.; Adachi, K.; Nishiyama, A. 1-nm Spatial Resolution in Carrier Profiling of Ultrashallow Junctions by Scanning Spreading Resistance Microscopy | IEEE Journals & Magazine | IEEE Xplore. *IEEE Electron Device Letters* **2008**, *29* (7). DOI: 10.1109/LED.2008.2000644.
(22) Eyben, P.; Denis, S.; Clarysse, T.; Vandervorst, W. Progress towards a physical contact model for scanning spreading resistance microscopy. *Materials Science and Engineering: B* **2003/09/15**, *102* (1-3). DOI: 10.1016/S0921-5107(03)00019-9.
(23) Eyben, P.; Seidel, F.; Hantschel, T.; Schulze, A.; Lorenz, A.; Castro, A. U. D.; Gestel, D. V.; John, J.; Horzel, J.; Vandervorst, W. Development and optimization of scanning spreading resistance microscopy for measuring the two-dimensional carrier profile in solar cell structures. *physica status solidi (a)* **2011/03/01**, *208* (3). DOI: 10.1002/pssa.201000306.

AIP Publishing Applied Physics Reviews ACCEPTED MANUSCRIPT
This is the author's peer reviewed, accepted manuscript. However, the online version of record will be different from this version once it has been copyedited and typeset.
PLEASE CITE THIS ARTICLE AS DOI: 10.1063/5.0280969

(24) De Wolf, P.; Stephenson, R.; Trenkler, T.; Clarysse, T.; Hantschel, T.; Vandervorst, W. Status and review of two-dimensional carrier and dopant profiling using scanning probe microscopy. *Journal of Vacuum Science & Technology B: Microelectronics and Nanometer Structures Processing, Measurement, and Phenomena* **2000/01/01**, *18* (1). DOI: 10.1116/1.591198.
(25) Oliver, R. A. Advances in AFM for the electrical characterization of semiconductors. *Reports on Progress in Physics* **2008**, *71* (7), 076501.
(26) Schulze, A.; Cao, R.; Eyben, P.; Hantschel, T.; Vandervorst, W. Outwitting the series resistance in scanning spreading resistance microscopy. *Ultramicroscopy* **2016**, *161*, 59-65. DOI: 10.1016/j.ultramic.2015.10.029.
(27) Eyben, P.; Bisiaux, P.; Schulze, a.; Nazir, a.; Vandervorst, W. Fast Fourier transform scanning spreading resistance microscopy: a novel technique to overcome the limitations of classical conductive AFM techniques. *Nanotechnology* **2015**, *26* (35), 355702-355702. DOI: 10.1088/0957-4484/26/35/355702.
(28) Qin, S.; Suo, Z.; Fillmore, D.; Lu, S.; Jeff Hu, Y.; McTeer, A. Ambient-controlled scanning spreading resistance microscopy measurement and modeling. *Applied Physics Letters* **2013/12/23**, *103* (26). DOI: 10.1063/1.4858963.
(29) Mody, J.; Kambham, A. K.; Eyben, P.; Schulze, A.; Hoffmann, T. y.; Vandervorst, W. Dopant and Carrier Profiling in FinFET-based devices with sub-nanometer resolution. **2010**, *26* (1), 195-196.
(30) Qin, S.; Qin, S. AC-SSRM 2-D Cross-Sectional Doping Profiling for DRAM Access Devices Contact Implants - R Discovery. *IEEE Transactions on Electron Devices* **2020-11-01**, *67* (11). DOI: 10.1109/ted.2020.3020525.
(31) Qin, S.; Hu, Y. J.; McTeer, A.; Fillmore, D.; Lu, S.; Burke, R.; Guha, J.; Vanhaeren, D.; Eyben, P.; Vandervorst, W. Two-Dimensional Cross-Sectional Doping Profile Study of Low Energy High Dose Ion Implantations Using High Vacuum Scanning Spreading Resistance Microscopy (HV-SSRM) and Electron Holography. *AIP Conference Proceedings* **2011/01/07**, *1321* (1). DOI: 10.1063/1.3548345.
(32) Eyben, P.; De Keersgieter, A.; Celano, U.; Wouters, L.; Chiarella, T.; Ritzenthaler, R.; Mertens, H.; Richard, O.; Paredis, K.; Matagne, P.; et al. Combining TCAD and advanced metrology techniques to support device integration towards N3. In *2021 20th International Workshop on Junction Technology (IWJT)*, 2021/6//, 2021; IEEE: pp 1-4. DOI: 10.23919/IWJT52818.2021.9609513.
(33) Eyben, P. Direct extraction of contact and S/D epi access resistance components on 45nm Gate Pitch NS-based n-FET devices for the 2nm node. In *2024 International Electron Devices Meeting (IEDM)*;, 2024. DOI: 10.1109/IEDM50854.2024.10873517.
(34) Nazir, A.; Spessot, A.; Eyben, P.; Clarysse, T.; Ritzenthaler, R.; Schram, T.; Vandervorst, W. Accurate Prediction of Device Performance Based on 2-D Carrier Profiles in the Presence of Extensive Mobile Carrier Diffusion. *IEEE Transactions on Electron Devices* **2014**, *61* (8), 2633-2639. DOI: 10.1109/TED.2014.2327759.
(35) Nazir, A. Scanning Spreading Resistance Microscopy for TCAD calibration in CMOS technologies, PhD thesis. **2015**.
(36) Mody, J.; Eyben, P.; Augendre, E.; Richard, O.; Vandervorst, W. Toward extending the capabilities of scanning spreading resistance microscopy for fin field-effect-transistor-based structures. *Journal of Vacuum Science & Technology B: Microelectronics and Nanometer Structures* **2008**, *26* (1), 351-351. DOI: 10.1116/1.2819254.
(37) Mody, J.; Zschätzsch, G.; Kölling, S.; Keersgieter, A. D.; Eneman, G.; Kambham, A. K.; Schulze, A.; Chiarella, T.; Horiguchi, N.; Hoffmann, T. y.; et al. 3D-Carrier Profiling in FinFETs using Scanning Spreading Resistance Microscopy. *IEDM Tech. Dig.* **2011**, 119-122.
(38) Celano, U.; Hsia, F.-C.; Vanhaeren, D.; Paredis, K.; Nordling, T. E. M.; Buijnsters, J. G.; Hantschel, T.; Vandervorst, W. Mesoscopic physical removal of material using sliding nano-diamond contacts. *Scientific Reports* **2018**, *8* (1), 2994-2994. DOI: 10.1038/s41598-018-21171-w.
(39) Celano, U.; Vandervorst, W. Scanning Probe Tomography for Advanced Material Characterization. *Integrated Reliability Workshop Final Report (IIRW), 2014 IEEE International* **2014**, 1-5.

AIP Publishing Applied Physics Reviews ACCEPTED MANUSCRIPT
This is the author's peer reviewed, accepted manuscript. However, the online version of record will be different from this version once it has been copyedited and typeset.
PLEASE CITE THIS ARTICLE AS DOI: 10.1063/5.0280969

(40) Song, J.; Zhou, Y.; Huey, B. D. 3D structure-property correlations of electronic and energy materials by tomographic atomic force microscopy. In *Applied Physics Letters*, American Institute of Physics Inc.: 2021; Vol. 118.
(41) Coq Germanicus, R.; Leclère, P.; Guhel, Y.; Boudart, B.; Touboul, A.; Descamps, P.; Hug, E.; Eyben, P. On the effects of a pressure induced amorphous silicon layer on consecutive spreading resistance microscopy scans of doped silicon. *Journal of Applied Physics* **2015**, *117* (24).
(42) Laskar, M. A. R.; Leonetti, G.; Milano, G.; Novotný, O.; Neuman, J.; Tongay, S.; Celano, U. Adaptive Scalpel Scanning Probe Microscopy for Enhanced Volumetric Sensing in Tomographic Analysis. *Advanced Materials Interfaces* **2024/07/01**, *11* (21). DOI: 10.1002/admi.202400187.
(43) Chen, S.; Jiang, L.; Buckwell, M.; Jing, X.; Ji, Y.; Grustan-Gutierrez, E.; Hui, F.; Shi, Y.; Rommel, M.; Paskaleva, A.; et al. On the Limits of Scalpel AFM for the 3D Electrical Characterization of Nanomaterials. *Advanced Functional Materials* **2018**, *1802266*, 1-15. DOI: 10.1002/adfm.201802266.
(44) Noël, C.; Wouters, L.; Paredis, K.; Celano, U.; Hantschel, T. Oil as an Enabler for Efficient Materials Removal in Three-Dimensional Scanning Probe Microscopy Applications. *Frontiers in Mechanical Engineering* **2021**, *7*. DOI: 10.3389/fmech.2021.797962.
(45) Jacobs, T. D. B.; Carpick, R. W. Nanoscale wear as a stress-assisted chemical reaction. *Nature nanotechnology* **2013**, *8* (2), 108-112. DOI: 10.1038/nnano.2012.255.
(46) Eyben, P.; Chiarella, T.; Kubicek, S.; Bender, H.; Richard, O.; Mitard, J.; Mocuta, A.; Horiguchi, N.; Thean, A. V.-Y. Scalpel soft retrace scanning spreading resistance microscopy for 3D-carrier profiling in sub-10nm WFIN FinFET | IEEE Conference Publication | IEEE Xplore. *2015 IEEE International Electron Devices Meeting (IEDM)* **2015**. DOI: 10.1109/IEDM.2015.7409693.
(47) Sharma, D.; Tedaldi, M.; Hole, P.; Humphris, A. D. L.; Wouters, L.; Hantschel, T.; Celano, U. An Innovative Multi-Probe Tomographic Atomic Force Microscope for Materials Research and Failure Analysis. *EDFA Technical Articles* **2023/11/01**, *25* (4). DOI: 10.31399/asm.edfa.2023-4.p020.
(48) Dixon-Luinenburg, O.; Celano, U.; Vandervorst, W.; Paredis, K. Carrier profiling with fast Fourier transform scanning spreading resistance microscopy: A case study for Ge, GaAs, InGaAs, and InP. *Ultramicroscopy* **2019**, *206*, 112809-112809. DOI: 10.1016/j.ultramic.2019.06.009.
(49) Lee, S.-Y.; Kim, S.-M.; Yoon, E.-J.; Oh, C. W.; Chung, I.; Park, D.; Kim, K. Three-dimensional MBCFET as an ultimate transistor | IEEE Journals & Magazine | IEEE Xplore. *IEEE Electron Device Letters* **2004**, *25* (4). DOI: 10.1109/LED.2004.825199.
(50) Kuhn, K. J. Considerations for Ultimate CMOS Scaling | IEEE Journals & Magazine | IEEE Xplore. *IEEE Transactions on Electron Devices* **2012**, *59* (7). DOI: 10.1109/TED.2012.2193129.
(51) Pandey, K.; Paredis, K.; Robson, A. J.; Vandervorst, W. Understanding the effect of confinement in scanning spreading resistance microscopy measurements. *Journal of Applied Physics* **2020**, *128* (3), 034303-034303. DOI: 10.1063/5.0011703.
(52) Eyben, P.; Fukutome, H.; Alvarez, D.; Vandervorst, W. High resolution two-dimensional carrier profiling on sub-100nm silicon nano-devices using scanning spreading resistance microscopy. In *Proceedings of the 30th European Solid-State Circuits Conference (IEEE Cat. No. 04EX850)*, 2004; IEEE: pp 101-104.
(53) Sibaja-Hernandez, A.; Eyben, P.; Van Huylenbroeck, S.; Vanhaeren, D.; Vandervorst, W.; Decoutere, S.; Maes, H. 2D-TCAD process calibration for a high speed QSA SiGe: C HBT verified with SSRM. *ECS Transactions* **2006**, *3* (7), 387.
(54) Ferrada, P.; Harney, R.; Wefringhaus, E.; Doering, S.; Jakschick, S.; Mikolajick, T.; Eyben, P.; Hantschel, T.; Vandervorst, W.; Weiss, M.; et al. Local Doping Profiles for Height-Selective Emitters Determined by Scanning Spreading Resistance Microscopy (SSRM) | IEEE Journals & Magazine | IEEE Xplore. *IEEE Journal of Photovoltaics* **2013**, *3* (1). DOI: 10.1109/JPHOTOV.2012.2213580.
(55) Weber, J.; Brand, A. A Scanning Spreading Resistance Microscopy Study on a Laser-Doped Selective Phosphorous Emitter | IEEE Journals & Magazine | IEEE Xplore. *IEEE Journal of Photovoltaics* **2020**, *10* (5). DOI: 10.1109/JPHOTOV.2020.3009567.

AIP Publishing Applied Physics Reviews ACCEPTED MANUSCRIPT
This is the author's peer reviewed, accepted manuscript. However, the online version of record will be different from this version once it has been copyedited and typeset.
PLEASE CITE THIS ARTICLE AS DOI: 10.1063/5.0280969

(56) Fırat, M.; Wouters, L.; Lagrain, P.; Haase, F.; Polzin, J.-I.; Chaudhary, A.; Nogay, G.; Desrues, T.; Krügener, J.; Peibst, R.; et al. Local Enhancement of Dopant Diffusion from Polycrystalline Silicon Passivating Contacts. *ACS Applied Materials & Interfaces* **April 5, 2022**, *14* (15). DOI: 10.1021/acsami.2c01801.
(57) Doering, S.; Rudolf, R.; Pinkert, M.; Roetz, H.; Wagner, C.; Eckl, S.; Strasser, M.; Wachowiak, A.; Mikolajick, T. Scanning spreading resistance microscopy for failure analysis of nLDMOS devices with decreased breakdown voltage. *Microelectronics Reliability* **2014/09/01**, *54* (9-10). DOI: 10.1016/j.microrel.2014.07.021.
(58) Song, X.; Michaud, J.; Cayrel, F.; Zielinski, M.; Portail, M.; Chassagne, T.; Collard, E.; Alquier, D. Evidence of electrical activity of extended defects in 3C–SiC grown on Si. *Applied Physics Letters* **2010**, *96* (14).
(59) Swanson, L.; Fiorenza, P.; Giannazzo, F.; Frazzetto, A.; Roccaforte, F. Correlating macroscopic and nanoscale electrical modifications of SiO2/4H-SiC interfaces upon post-oxidation-annealing in N2O and POCl3. *Applied Physics Letters* **2012**, *101* (19).
(60) Schulze, A.; Verhulst, A. S.; Nazir, A.; Hantschel, T.; Eyben, P.; Vandervorst, W. A comprehensive model for the electrical nanocontact on germanium for scanning spreading resistance microscopy applications. *Journal of Applied Physics* **2013/03/21**, *113* (11). DOI: 10.1063/1.4795141.
(61) Lu, R. P.; Kavanagh, K. L.; Dixon-Warren, S. J.; Kuhl, A.; Thorpe, A. J. S.; Griswold, E.; Hillier, G.; Calder, I.; Ares, R.; Streater, R. Calibrated scanning spreading resistance microscopy profiling of carriers in III-V structures. *Journal of Vacuum Science & Technology B* **2001**, *19* (4), 1662-1670. DOI: 10.1116/1.1387458.
(62) Hsieh, P.-Y.; O'Sullivan, B.; Tsiara, A.; Truijen, B.; Lagrain, P.; Wouters, L.; Yudistira, D.; Kunert, B.; Campenhout, J. V.; Wolf, I. D. Advanced Current–Voltage Model of Electrical Contacts to GaAs- and Ge-Based Active Silicon Photonic Devices | IEEE Journals & Magazine | IEEE Xplore. *IEEE Transactions on Electron Devices* **2023**, *70* (8). DOI: 10.1109/TED.2023.3285711.
(63) Xu, M. W.; Hantschel, T.; Vandervorst, W. Three-dimensional carrier profiling of InP-based devices using scanning spreading resistance microscopy. *Applied Physics Letters* **2002**, *81* (1), 177-177. DOI: 10.1063/1.1490399.
(64) Xu, M. W.; Hantschel, T.; Vandervorst, W. Three-dimensional carrier profiling of InP-based devices using scanning spreading resistance microscopy. *Applied Physics Letters* **2002**, *81* (1), 177-179. DOI: 10.1063/1.1490399.
(65) Nagpure, S. C.; Bhushan, B.; Babu, S.; Rizzoni, G. Scanning spreading resistance characterization of aged Li-ion batteries using atomic force microscopy. *Scripta Materialia* **2009**, *60* (11), 933-936.
(66) De Koninck, Y.; Caer, C.; Yudistira, D.; Baryshnikova, M.; Sar, H.; Hsieh, P.-Y.; Özdemir, C. I.; Patra, S. K.; Kuznetsova, N.; Colucci, D.; et al. GaAs nano-ridge laser diodes fully fabricated in a 300-mm CMOS pilot line. *Nature 2025 637:8044* **2025-01-01**, *637* (8044). DOI: 10.1038/s41586-024-08364-2.
(67) Coq Germanicus, R.; Othman, E.-H. Machine learning for predicting DataCube atomic force microscope (AFM)—MultiDAT-AFM. In *International Symposium for Testing and Failure Analysis*, 2024; ASM International: Vol. 84918, pp 351-357.
(68) Sumner, J.; Oliver, R. A.; Kappers, M. J.; Humphreys, C. J. Assessment of scanning spreading resistance microscopy for application to n-type GaN. *physica status solidi c* **2008/05/01**, *5* (6). DOI: 10.1002/pssc.200778569.
(69) Kaltsounis, T.; Haas, H.; Lafossas, M.; Torrengo, S.; Maurya, V.; Buckley, J.; Mariolle, D.; Veillerot, M.; Gueugnot, A.; Mendizabal, L.; et al. Characterization of unintentional doping in localized epitaxial GaN layers on Si wafers by scanning spreading resistance microscopy. *Microelectronic Engineering* **2023/03/15**, *273*. DOI: 10.1016/j.mee.2023.111964.
(70) Aiso, T.; Ichikawa, Y.; Yamashita, Y.; De Wolf, P.; Stephenson, R.; Trenkler, T.; Clarysse, T.; Hantschel, T.; Vandervorst, W. Status and review of two-dimensional carrier and dopant profiling using scanning probe microscopy. *Journal of Vacuum Science & Technology B: Microelectronics and Nanometer Structures* **2000**, *18* (1), 361-361. DOI: 10.1116/1.591198.

AIP Publishing Applied Physics Reviews ACCEPTED MANUSCRIPT
This is the author's peer reviewed, accepted manuscript. However, the online version of record will be different from this version once it has been copyedited and typeset.
PLEASE CITE THIS ARTICLE AS DOI: 10.1063/5.0280969

(71) SINGH, Y. ELECTRICAL RESISTIVITY MEASUREMENTS: A REVIEW. *International Journal of Modern Physics: Conference Series* **2013-05-26**, *22*. DOI: 10.1142/S2010194513010970.
(72) Pandey, K.; Paredis, K.; Hantschel, T.; Drijbooms, C.; Vandervorst, W. The impact of focused ion beam induced damage on scanning spreading resistance microscopy measurements. *Scientific Reports* **2020**, *10* (1). DOI: 10.1038/s41598-020-71826-w.
(73) Schulze, A.; Verhulst, A. S.; Nazir, A.; Hantschel, T.; Eyben, P.; Vandervorst, W. A comprehensive model for the electrical nanocontact on germanium for scanning spreading resistance microscopy applications. *Journal of Applied Physics* **2013**, *113* (11), 114310-114310. DOI: 10.1063/1.4795141.
(74) Vandervorst, W.; Fleischmann, C.; Bogdanowicz, J.; Franquet, A.; Celano, U.; Paredis, K.; Budrevich, A. Dopant, composition and carrier profiling for 3D structures. *Materials Science in Semiconductor Processing* **2017**, *62* (July), 31-48. DOI: 10.1016/j.mssp.2016.10.029.
(75) Adlmaier, T.; Doering, S.; Binder, B.; Simon, D.; Mikolajick, T.; Eng, L. Improved 2D charge carrier quantification workflow for scanning spreading resistance microscopy. *Microelectronics Reliability* **2025**, *168*, 115646.
(76) Wouters, L.; Peters, K.; Lagrain, P.; Drees, R.; Peric, N.; Hantschel, T. Leveraging Artificial Intelligence and Reverse Tip Sample Configuration for Automation of Data Processing in Quantitative Scanning Spreading Resistance Microscopy. *physica status solidi (a)* **2024**. DOI: 10.1002/pssa.202400688.
(77) Rahman Laskar, M. A.; Celano, U. Scanning probe microscopy in the age of machine learning. *APL Machine Learning* **2023**, *1* (4).
(78) Krull, A.; Hirsch, P.; Rother, C.; Schiffrin, A.; Krull, C. Artificial-intelligence-driven scanning probe microscopy. *Communications Physics* **2020**, *3* (1), 54.
(79) Pürckhauer, K.; Weymouth, A. J.; Pfeffer, K.; Kullmann, L.; Mulvihill, E.; Krahn, M. P.; Müller, D. J.; Giessibl, F. J.; Pürckhauer, K.; Weymouth, A. J.; et al. Imaging in Biologically-Relevant Environments with AFM Using Stiff qPlus Sensors. *Scientific Reports 2018 8:1* **2018-06-19**, *8* (1). DOI: 10.1038/s41598-018-27608-6.
(80) C, X.; X, X.; X, H.; H, W.; L, C.; SH, K.; L, Q. Surface Structure Dependence of Mechanochemical Etching: Scanning Probe-Based Nanolithography Study on Si(100), Si(110), and Si(111) - PubMed. *ACS applied materials & interfaces* **06/12/2019**, *11* (23). DOI: 10.1021/acsami.9b00133.
(81) Eyben, P.; De Keersgieter, A.; Celano, U.; Wouters, L.; Chiarella, T.; Ritzenthaler, R.; Mertens, H.; Richard, O.; Paredis, K.; Matagne, P. Combining TCAD and advanced metrology techniques to support device integration towards N3. In *2021 20th International Workshop on Junction Technology (IWJT)*, 2021; IEEE: pp 1-4.
(82) Celano, U.; Paredis, K.; Humphris, A.; Tedaldi, M.; O'Sullivan, C.; Hole, P.; Goulden, J. An innovative probe microscopy solution for measuring conductivity profiles in 3-dimensions. In *Metrology, Inspection, and Process Control for Semiconductor Manufacturing XXXV*, 2021/2//, 2021; Adan, O., Robinson, J. C., Eds.; SPIE: pp 13-13. DOI: 10.1117/12.2583065.
(83) Kim, H.-S.; Peric, N.; Minj, A.; Wouters, L.; Serron, J.; Mancini, C.; Koylan, S.; Sergeant, S.; Hantschel, T.; Kim, H.-S.; et al. Probe chip nanofabrication enabled reverse tip sample scanning probe microscopy concept and measurements. *Nanotechnology* **2024-04-09**, *35* (26). DOI: 10.1088/1361-6528/ad3744.
(84) Lagrain, P.; Paulussen, K.; Grieten, E.; Bosch, G. V. d.; Rachidi, S.; Yudistira, D.; Wouters, L.; Hantschel, T. Enabling focused ion beam sample preparation for application in reverse tip sample scanning probe microscopy. *Micro and Nano Engineering* **2024/06/01**, *23*. DOI: 10.1016/j.mne.2024.100247.
(85) De Wolf, P.; Snauwaert, J.; Hellemans, L.; Clarysse, T.; Vandervorst, W.; D'Olieslaeger, M.; Quaeyhaegens, D. Lateral and vertical dopant profiling in semiconductors by atomic force microscopy using conducting tips. *Journal of Vacuum Science & Technology A* **1995/05/01**, *13* (3). DOI: 10.1116/1.579754.

AIP Publishing Applied Physics Reviews ACCEPTED MANUSCRIPT
This is the author's peer reviewed, accepted manuscript. However, the online version of record will be different from this version once it has been copyedited and typeset.
PLEASE CITE THIS ARTICLE AS DOI: 10.1063/5.0280969

(86) Niedermann, P.; Hänni, W.; Blanc, N.; Christoph, R.; Burger, J. Chemical vapor deposition diamond for tips in nanoprobe experiments. *Journal of Vacuum Science & Technology A* **1996/05/01**, *14* (3). DOI: 10.1116/1.580273.
(87) Oesterschulze, E.; Scholz, W.; Mihalcea, C.; Albert, D.; Sobisch, B.; Kulisch, W. Fabrication of small diamond tips for scanning probe microscopy application. *Applied Physics Letters* **1997/01/27**, *70* (4). DOI: 10.1063/1.118173.
(88) Hantschel, T.; Niedermann, P.; Trenkler, T.; Vandervorst, W. Highly conductive diamond probes for scanning spreading resistance microscopy. *Applied Physics Letters* **2000**, *76* (12), 1603-1603. DOI: 10.1063/1.126109.
(89) Schulze, A.; Hantschel, T.; Dathe, A.; Eyben, P.; Ke, X.; Vandervorst, W. Electrical tomography using atomic force microscopy and its application towards carbon nanotube-based interconnects. *Nanotechnology* **2012**, *23* (30), 305707-305707. DOI: 10.1088/0957-4484/23/30/305707.
(90) *Electrical Atomic Force Microscopy for Nanoelectronics*; Springer International Publishing, 2019. DOI: 10.1007/978-3-030-15612-1.
(91) Hantschel, T.; Clarysse, T.; Ajaykumar, A.; Seidel, F.; Tsigkourakos, M.; Nuytten, T.; Paredis, K.; Eyben, P.; Majeed, B.; Tezcan, D. S.; et al. Diamond nanoprobes for electrical probing of nanoelectronics device structures. *Microelectronic Engineering* **2014/06/01**, *121*. DOI: 10.1016/j.mee.2014.02.024.
(92) Hantschel, T.; Tsigkourakos, M.; Kluge, J.; Werner, T.; Zha, L.; Paredis, K.; Eyben, P.; Nuytten, T.; Xu, Z.; Vandervorst, W. Overcoated diamond tips for nanometer-scale semiconductor device characterization. *Microelectronic Engineering* **2015/06/15**, *141*. DOI: 10.1016/j.mee.2014.11.023.
(93) Wouters, L.; Boehme, T.; Mana, L.; Hantschel, T. Self-patterned ultra-sharp diamond tips and their application for advanced nanoelectronics device characterization by electrical SPM. *Micro and Nano Engineering* **2023/06/01**, *19*. DOI: 10.1016/j.mne.2023.100195.
(94) Tsigkourakos, M.; Hantschel, T.; Arstila, K.; Vandervorst, W. Diamond nano-particle seeding for tip moulding application. *Diamond and Related Materials* **2013**, *35*, 14-18. DOI: 10.1016/j.diamond.2013.03.008.
(95) Buijnsters, J. G.; Tsigkourakos, M.; Hantschel, T.; Gomes, F. O. V.; Nuytten, T.; Favia, P.; Bender, H.; Arstila, K.; Celis, J.-P.; Vandervorst, W. Effect of Boron Doping on the Wear Behavior of the Growth and Nucleation Surfaces of Micro and Nanocrystalline Diamond Films. *ACS Applied Materials & Interfaces* **2016**, acsami.6b08083-acsami.08086b08083. DOI: 10.1021/acsami.6b08083.
(96) Wouters, L.; Cho, J.; Gim, S.; Yang, J.; Kanniainen, A.; Lee, K.; Lagrain, P.; Peric, N.; Hantschel, T. Nanofabrication of sharp conductive diamond tip probe chips and their application in reverse tip sample scanning probe microscopy. *Micro and Nano Engineering* **2025**, 100307.